Production of human papillomavirus type 16 virus-like particles in Physcomitrella photobioreactors

Paul Alexander Niederau[1], Maria Caroline Weilguny[1,2], Sarah Chamas[1], Caitlin Elizabeth Turney[1], Juliana Parsons[1], Marta Rodríguez-Franco[3], Sebastian N.W. Hoernstein[1], Eva L. Decker[1], Henrik Toft Simonsen[2,4], Ralf Reski[1,5,6 *]

[1] Plant Biotechnology, Faculty of Biology, University of Freiburg, Schänzlestr. 1, 79104 Freiburg, Germany

[2] Department of Biotechnology and Biomedicine, Technical University of Denmark, 2800 Kongens Lyngby, Denmark

[3] Cell Biology, Faculty of Biology, University of Freiburg, Schänzlestr. 1, 79104 Freiburg, Germany

[4] Laboratoire de Biotechnologies Végétales appliquées aux Plantes Aromatiques et Médicinales, CNRS, UMR 5079, Université Jean Monnet, 42023 Saint-Etienne Cedex 2, France

[5] Signalling Research Centre BIOSS and CIBSS, University of Freiburg, Schänzlestr. 18, 79104 Freiburg, Germany

[6] Cluster of Excellence *liv*MatS @ FIT – Freiburg Centre for Interactive Materials and Bioinspired Technologies, University of Freiburg, Georges-Köhler-Allee 105, 79110 Freiburg, Germany

*Corresponding author: ralf.reski@biologie.uni-freiburg.de

ORCID

P.A.N.	0009-0004-0194-8570
M.C.W.	0009-0009-9440-6872
S.C.	0009-0007-5704-5639
C.E.T.	0009-0001-3113-4648
J.P.	0000-0001-6261-2342
M.R.F.	0000-0003-1183-2075
S.N.W.H.	0000-0002-2095-689X
E.L.D.	0000-0002-9151-1361
H.T.S.	0000-0003-3070-807X
R.R.	0000-0002-5496-6711

Author E-mails

P.A.N.	alexander.niederau@biologie.uni-freiburg.de
M.C.W.	mariaweilguny@gmail.com
S.C.	sarah-chamas@web.de
C.E.T.	caitlin.turney@email.uni-freiburg.de
J.P.	juliana.parsons@biologie.uni-freiburg.de
M.R.F.	marta.rodriguez@biologie.uni-freiburg.de
S.N.W.H.	sebastian.hoernstein@biologie.uni-freiburg.de
E.L.D.	eva.decker@biologie.uni-freiburg.de
H.T.S.	henrik.toft.simonsen@univ-st-etienne.fr
R.R.	ralf.reski@biologie.uni-freiburg.de

Word count: 7830

Figures: 6

Tables: 1

Abstract

Virus-like particles (VLPs) are self-assembling nanoparticles composed of viral structural proteins which mimic native virions but lack viral DNA and infectivity. VLPs are a resourceful class of biopharmaceuticals applied as subunit vaccines or as delivery vehicles for drugs and nucleic acids. Similar to viruses, VLPs are diverse in structure, composition, and assembly, requiring a tailored production platform aligned with the intended application. The moss plant Physcomitrella (*Physcomitrium patens*) is an emerging expression system offering humanized N-glycosylation, scalability, and adaptability to existing industry settings. Here, we used Physcomitrella to produce human papillomavirus (HPV) 16 VLPs. HPV VLPs are composed of the major structural protein L1 and are used as vaccines against HPV infections which are the main causal agent of cervical and other anogenital cancers. We characterized Physcomitrella chloroplast transit peptides, which we used for targeting of moss-produced L1 to chloroplasts, leading to higher recombinant protein yield compared to nuclear or cytoplasmic localization. We confirmed subcellular localization with confocal laser scanning microscopy and found L1 to accumulate within the chloroplast stroma. Production in 5-liter photobioreactors yielded over 0.3 mg L1 per gram fresh weight. We established a purification protocol for moss-produced L1 using a combination of ammonium sulfate precipitation and cation exchange chromatography. Purified samples were subjected to a controlled dis- and reassembly, yielding fully assembled HPV-16 L1 VLPs. This is the first report of production, purification, and assembly of VLPs in a non-vascular plant.

Keywords: bryophyte, bioreactor, molecular farming, nanoparticle, plant biotechnology, vaccine candidate

Key message: First production of virus-like particles as a vaccine candidate in a non-vascular plant.

72 ## Introduction

73 Virus-like particles (VLPs) are nanoparticles consisting of viral structural proteins (Marsian and
74 Lomonossoff, 2016; Nooraei et al., 2021). VLPs cannot replicate and infect cells, but resemble native
75 viruses in size, shape, and surface structure, presenting highly repetitive immunogenic epitopes. As a
76 result, VLPs have a wide range of applications as vaccines and nanocarriers and are of high interest in
77 biopharmaceutical research and development.

78 There is currently a range of VLP-based vaccines licensed and available against infectious diseases
79 such as hepatitis B, hepatitis E, human papillomavirus (HPV), malaria, and human Norwalk virus with many
80 more vaccine candidates in clinical trials (Nooraei et al., 2021; Gupta et al., 2023). Viral capsid proteins
81 stimulate both the cellular and the humoral immune response, leading to the generation of cytotoxic and
82 memory T cells as well as the production of specific antibodies *via* B cells (Ross et al., 2009; Song et al.,
83 2011; Serradell et al., 2019; Chi et al., 2024). VLP-based vaccines offer improved safety as compared to
84 live-attenuated or inactivated vaccines, which carry the risk of reverting to a pathogenic form (Burns et
85 al., 2014). At the same time, VLPs don't suffer the limitations of DNA-based vaccines, including risk of
86 genome integration or of appropriate delivery which ultimately lowers immunogenicity (Lu et al., 2024).
87 VLPs are not only used for their intrinsic antigenic properties but serve as nanoparticles for drug delivery
88 by loading their inner space with cargo such as nucleic acids (Lamprecht et al., 2016; Adams et al., 2023).
89 Besides the inner space, VLPs can also be used to display antigens on the capsid's surface. For the
90 treatment of pancreatic cancers, disease-unrelated VLPs were coated with respective antigens and were
91 demonstrated to inhibit cancer growth (Cubas et al., 2011; Zhang et al., 2013). Yet, empty VLPs of Cowpea
92 Mosaic Virus, a rod-like shaped plant virus, were shown to reduce cancer growth, despite the absence of
93 disease-specific antigens in the vaccine (Lizotte et al., 2015). The ability of VLPs to induce strong T cell-
94 mediated immune responses is essential in VLP-based cancer vaccines (Nooraei et al., 2021). Overall, VLPs
95 possess characteristics that make them highly versatile for applications in vaccine development, targeted
96 drug delivery, gene therapy, and immunotherapy, offering significant potential in modern biomedicine.

97 VLPs are classified based on various structural characteristics, one of which is the presence or
98 absence of a lipid envelope (Nooraei et al., 2021). In enveloped VLPs (eVLPs) the viral capsid proteins are
99 imbedded within a lipid membrane acquired during particle assembly, typically from intracellular
100 membranes in the secretory pathway or the outer plasma membrane. Additional structural characteristics
101 include the number and types of capsid proteins, as well as their organization into single, double, or triple-
102 layered architectures. In some instances, capsid proteins require proteolytic processing or N-glycosylation

103 to enable budding of assembled particles from the host cell's membrane and acquisition of the lipid
104 envelope (Welsch et al., 2007; Zlotnick and Mukhopadhyay, 2011; Kim et al., 2014). Furthermore, viral
105 antigens displayed on the surface of the lipid membrane are often glycosylated, which significantly
106 contributes to the immunogenicity of eVLP-based vaccines (Mortola and Roy, 2004). One example is the
107 major glycoprotein of Ebola virus for which the distinct glycosylation pattern is crucial for the formation
108 of neutralizing antibodies (Peng et al., 2022). Other notable cases include hepatitis C virus and Zika virus
109 – both of which currently lack a licensed vaccine – where the induction of neutralizing antibodies depends
110 on viral glycoproteins (Torresi, 2017; Hasan et al., 2018). Consequently, the choice of VLP, its structural
111 complexity, and intended application play a crucial role in determining the appropriate expression system
112 and guiding cell line development.

113 The moss Physcomitrella has emerged as an alternative for biopharmaceutical production,
114 offering several advantages over traditional systems (Reski et al., 2015; Reski, 2018; Decker and Reski,
115 2020). Its haploid dominant phase and high rate of homologous recombination enable precise gene
116 targeting (Strepp et al., 1998; Wiedemann et al., 2018; Rempfer et al., 2022). This feature facilitated the
117 modification of the N-glycosylation pathway, eliminating plant-specific modifications, such as β1,2-
118 xylosylation, α1,3-fucosylation, and Lewis A epitopes (Koprivova et al., 2004; Parsons et al., 2012; Decker
119 et al., 2014). Moreover, enzymes necessary for sialic acid synthesis, activation, and linkage to protein N-
120 glycans were introduced (Bohlender et al., 2020; Bohlender et al., 2022). These modifications have
121 resulted in more homogeneous and human-like N-glycan structures on recombinant proteins. The
122 potential of Physcomitrella as a biopharmaceutical production platform is demonstrated by several
123 products in development. For example, moss-produced α-galactosidase A has successfully completed
124 clinical phase Ib (Shen et al., 2016; Hennermann et al., 2019). Other moss-produced proteins include
125 human factor H (FH) and synthetic FH-related multitarget regulators MFHR1 and MFHR13, which are
126 potential treatments for complement-related disorders (Büttner-Mainik et al., 2011; Michelfelder et al.,
127 2017, 2018; Top et al., 2019; Ruiz-Molina et al., 2022a) such as age-dependent macular degeneration
128 (Hector et al., 2025). Factor H produced in other systems faced difficulties in its application, such as *Pichia*
129 *pastoris*-produced factor H exhibiting non-optimal glycosylation and reduced half-life (Schmidt et al.,
130 2011; Kerr et al., 2021). Importantly, Physcomitrella cultivation in photobioreactors is tightly controlled
131 (Hohe et al., 2002), and thus compliant with Good Manufacturing Practice (GMP) standards, ensuring
132 high-quality production of recombinant proteins (Reski et al., 2018; Decker and Reski, 2020). As opposed
133 to transiently transfected *Nicotiana benthamiana* plants cultivated in green houses, cultivation of stable
134 transgenic Physcomitrella cell lines in bioreactors is more in line with current production processes

135 applied in industry, thereby facilitating adaption to industry settings (Benvenuto et al., 2023). In addition,
136 cultivation of plant material in bioreactors allows greater scalability, which is a relevant aspect in
137 transitioning to industrial scale production. The company Medicago, focusing on VLP production in
138 transiently transfected *N. benthamiana*, announced challenges in transitioning with their platform to
139 industrial scale production as a reason for seizing further operations in 2023 (Mitsubishi Chemical Group
140 Corporation, 2023). In contrast, the company Eleva upscaled protein production in Physcomitrella from
141 200 L single-use bioreactors (Niederkrüger et al., 2019) to 1000 L photobioreactors (Eleva, 2025). In
142 summary, Physcomitrella is an ideal production host for complex biopharmaceuticals, including viral
143 antigens or glycosylated proteins, with great prospects regarding scalability and transition to industrial
144 production (Rosales-Mendoza et al., 2014). The first moss-produced vaccine candidate, an ENV-derived
145 multi-epitope HIV chimeric protein, was immunogenic in mice (Orellana-Escobedo et al., 2015). However,
146 until now, there was no record of VLP-production in Physcomitrella, or any other non-vascular plant.

147 VLPs of the human papillomavirus (HPV) are of great medicinal relevance due to their use as
148 vaccines to prevent HPV infection. HPV infections are a major source of cancer, causing approximately
149 690,000 cases annually (zur Hausen et al., 1981; zur Hausen, 2002; de Martel et al., 2020). The most
150 prevalent type is cervical cancer, accounting for about 80% of HPV-attributable cancers. Other HPV-
151 related cancers include anogenital and oropharyngeal cancers (Wu et al., 2024). HPV belongs to the
152 *Papillomaviridae*, comprising nearly 200 different types, which are commonly transmitted sexually
153 (Ljubojevic and Skerlev, 2014). The majority of HPV-attributable cancers are linked to two types in
154 particular, namely HPV-16 and HPV-18 (de Martel et al., 2020; Wu et al., 2024). HPV is a non-enveloped
155 double stranded DNA virus with a genome size of 8000 bp, encoding six early regulatory proteins (E1, E2,
156 E4 – E7) and two late structural proteins (L1, L2) (Roden and Stern, 2018). L1 proteins multimerize into
157 pentamers, the capsomers, and L1 capsomers and L2 monomers are imported into the nucleus *via* nuclear
158 localization signals (NLS), where HPV virions assemble (Cerqueira and Schiller, 2017). The final HPV-16
159 virion is composed of 360 L1 monomers, organized in 72 pentamers, and 72 L2 monomers and is
160 reinforced by inter-pentameric disulfide bonds (Baker et al., 1991; Buck et al., 2005). While the role of L2
161 in virion assembly differs from type to type, L1 can self-assemble into VLPs in the absence of L2 (Kirnbauer
162 et al., 1992). HPV L1 VLPs are mono-layered and do not contain a lipid envelope. Because the viral life
163 cycle depends on differentiated epithelial cells, it is difficult to obtain large quantities of virions. Therefore,
164 current HPV vaccines are based on L1 VLPs. Although VLP-based HPV vaccines are currently produced in
165 *Escherichia coli*, *Saccharomyces cerevisiae*, and baculovirus-infected insect cells (World Health

166 Organization, 2024), plant-based expression systems are gaining attention in this respect (Scotti and
167 Rybicki, 2013; Rybicki, 2020).

168 While first attempts to produce L1-based VLPs in plants had low yields (Biemelt et al., 2003;
169 Varsani et al., 2003), considerable improvements have been achieved, e.g. by codon optimization and
170 subcellular targeting strategies in transiently transformed tobacco (Maclean et al., 2007). A human codon-
171 optimized version (62% GC content) resulted in highest yields as compared to *N. benthamiana* optimized
172 (49% GC) and the native sequence (37% GC), presumably not due to the GC content but due to inhibitory
173 5' sequences, which act on transcription and mRNA processing (Maclean et al., 2007; Hitzeroth et al.,
174 2018). Further, these authors found chloroplast-targeted L1 yield highest at 0.5 mg / g fresh weight (FW)
175 followed by cytoplasmic L1 (without the C-terminal 22 aa NLS), whereas L1 targeted to the ER was not
176 detectable. Similarly, Zahin et al. (2016) reported 0.25 mg L1 / g FW *via* chloroplast targeting while leaving
177 the NLS intact. Although *N. benthamiana* remains a prominent option, other plants are increasingly
178 explored for the efficient production of biopharmaceuticals.

179 Here, we analyzed the expression of HPV-16 L1 in Physcomitrella. We characterized five
180 Physcomitrella chloroplast transit peptides and investigated the effect of subcellular L1 localization on
181 recombinant protein yields. We further established L1 production in photobioreactors and subsequent
182 purification of the product. Finally, the assembly of moss-produced HPV-16 L1 to VLPs was demonstrated
183 with transmission electron microscopy. Our goal was to obtain proof-of-concept to produce a simple but
184 medicinally relevant VLP before progressing towards more complex targets such as eVLPs consisting of
185 multiple proteins and layers.

186

187 ## Materials and methods

188 ### Plant material

189 Physcomitrella (new species name: *Physcomitrium patens* (Hedw.) Mitt.; IMSC accession number
190 41269), was cultivated according to Reski and Abel (1985) and Decker et al. (2015).

191

192 ### Optimization of HPV-L16 L1 coding sequence

193 The coding sequence (CDS) of h(human codon-optimized)L1 (GenBank acc. no. DQ067889,
194 Maclean et al., 2007) was used for optimization using physCO (https://www.plant-biotech.uni-

195 freiburg.de/tools/physco/; Top et al., 2021). Putative alternative splicing motifs AGGT were identified *via*
196 search function. MicroRNA-binding sites were predicted *via* psRNATarget with the library of 280 published
197 Physcomitrella microRNAs and the default settings *Schema V2* (2017 release)
198 (http://plantgrn.noble.org/psRNATarget/; Dai and Zhao, 2011; Dai et al., 2018). Alternative splice sites
199 and microRNA-binding sites were removed and substituted by synonymous codons based on
200 http://www.kazusa.or.jp/codon/. Sequence editing was done in Benchling
201 (https://www.benchling.com/).
202

203 **Expression vectors**

204 Chloroplast transit peptides (CTPs) were selected from a list of proteins with experimentally
205 confirmed cleavage of a predicted CTP (Hoernstein et al., 2024). CTP-eGFP vectors were constructed based
206 on a vector containing an eGFP CDS with an N-terminal linker (sequence: GGGGGA) under control of the
207 PpActin5 promoter (Weise et al., 2006) and nos terminator (Hoernstein et al., 2023). CTP candidates were
208 amplified from Physcomitrella cDNA and inserted at the N-terminus of the linker using Gibson Assembly
209 (Gibson et al., 2009). The Citrine-L1 fusion constructs are based on a vector containing the PpActin5
210 promoter, nos terminator and citrine CDS (Wiedemann et al., 2018). The CDS of pL1, pL1Δ22 and CTP-pL1
211 were amplified using Phusion™ polymerase (Thermo Fisher Scientific, Waltham, USA), cloned into the
212 pJet1.2 backbone (Thermo Fisher Scientific) and ligated into the expression vector using T4 Ligase (Thermo
213 Fisher Scientific), *via Xho*I and *BamH*I sites. The pL1 expression vectors were constructed based on a vector
214 containing the PpActin5 promoter, nos terminator and hpt cassette (Ruiz-Molina et al., 2022a). The pL1
215 sequence was synthesized by Genewiz (Leipzig, Germany). For constructs pL1 and pL1Δ22, the pL1 CDS
216 was amplified using Phusion™ polymerase (Thermo Fisher Scientific) and cloned as described above. For
217 construct CTP-pL1, the pL1 and CTPc5 CDS were amplified and inserted into the backbone using Gibson
218 Assembly. Vectors were sequenced by Eurofins Genomics (Ebersberg, Germany). Vector maps are
219 compiled in **Supplementary Figure S1**. Primers were synthesized by Eurofins Genomics and are compiled
220 in **Supplementary Table S1**.
221

222 **Protoplast preparation and transformation**

223 Physcomitrella protoplasts were prepared and transformed based on existing protocols (Hohe
224 and Reski, 2002; Schween et al., 2003; Hohe et al., 2004; Decker et al., 2015). Transformed protoplasts
225 were incubated at 22 °C for 24 h in the dark and subsequently for 72 h at a 16/8-h light/dark photoperiod

226 and light intensity of 50–70 µmol m^{-2} s^{-1} before plating on KnopME + 25 mg/L hygromycin agar plates
227 covered with cellophane for two weeks. Surviving colonies were transferred to non-selective conditions
228 for two weeks before a second selection on KnopME + 50 mg/L hygromycin.
229

230 **Fluorescence microscopy**

231 Protoplasts were analyzed 2-3 days after transfection with an AxioCam MRc5 camera on an
232 Axioplan2 stereo microscope (Zeiss, Oberkochen, Germany). Pictures were taken with a 40x objective or
233 a 63x objective with immersion oil. A FITC filter was used for eGFP, a rhodamine filter for chlorophyll
234 autofluorescence, and a FITC_LP filter for the combination of the two. Images were edited with GIMP
235 2.10.22 and ImageJ. For confocal microscopy, an AXIO Observer.Z1 Inverted Fluorescence Motorized
236 Phase Contrast Microscope Pred 7 with the objective Plan-Apochromat 63x/1.4 Oil DIC M27 (Zeiss) was
237 used. EGFP signals were detected at 488 / 509 nm, and chlorophyll autofluorescence at 587 / 610 nm.
238 Images were edited in ZEN 3.5 (Blue edition, ZEN Lite), ImageJ, and GIMP 2.10.22.
239 For analysis of subcellular targeting, an inverted confocal laser scanning microscope LSM 880 with
240 the objective LD LCI Plan-Apochromat 40x/1.2 H_2O autocorr and FastAiryScan mode (Zeiss) was used.
241 Citrine signals were detected at 488 / 516 nm, and chlorophyll autofluorescence at 561 / 595 nm. Images
242 were edited in ZEN 3.9 (Blue edition) and processed *via* deconvolution using default setting and
243 orthogonal projection using maximum intensity projection.
244

245 **Biomass accumulation**

246 Flasks containing 30 mL KnopME medium were inoculated at a density of 60 mg dry weight (DW)/L
247 and cultured for 4 weeks at the conditions described above. Biomass DW was measured by filtering 3x 10
248 mL of culture through miracloth and subsequent drying at 105 °C for 2 hours. Biomass accumulation was
249 analyzed by linear regression analysis. Slopes were compared using ANCOVA and post hoc multiple
250 comparisons test (TukeyHSD). The analysis was conducted in RStudio (version 4.2.2) and GraphPad Prism
251 (version 8.1).
252

253 **Bioreactor operation**

254 Stirred tank bioreactors (Getinge, Sweden) were inoculated at 60 mg DW/L moss density in 5 L
255 KnopME. The light intensity was set to 160 µmol m^{-2} s^{-1} and increased to 350 µmol m^{-2} s^{-1} after 4 days. At
256 day 4, auxin 1-Naphtalene acetic acid (NAA, Sigma, St. Louis, USA) dissolved in 0.5 M KOH was added to a

257 final concentration of 5 µM. Throughout the bioreactor run, the pH was kept at pH 5.8, temperature at
258 22 °C, and aeration at 0.3 vvm (volume air per volume media per minute) with 2% CO_2. The culture was
259 continuously agitated with a pitched 3 blade impeller at 500 rpm.
260

261 **Protein extraction, purification and VLP assembly**

262 For small scale extraction, 30 – 60 mg fresh weight (FW) of vacuum-filtered moss material was
263 combined with a glass and a steel bead (each 3 mm in diameter) in a 2 mL reaction tube, frozen in liquid
264 nitrogen and the tissue lysed using a tissue lyser for 2 min at 28 Hz. Homogenized material was
265 resuspended in PBS (2.7 mM KCl, 10 mM Na_2HPO_4, 1.8 mM KH_2PO_4, 0.137 M NaCl, pH 7.2), 0.01% (v/v)
266 Tween20, and protease inhibitor (P9599, Sigma) in a ratio 3 mL/g. Samples were placed in an ice-cold
267 sonication bath for 15 min, centrifuged for 30 min at 14,000 x g and 4 °C, and the supernatant taken off
268 for further analysis.
269 For large scale protein extraction, 5 g FW of vacuum-filtered moss material were frozen in liquid
270 nitrogen and ground to a fine powder. The material was combined with 22 mL PBS and 0.01% (v/v)
271 Tween20, 50 mM DTT and 100 µL protease inhibitor. The mixture was homogenized using an ULTRA-
272 TURRAX (IKA, Staufen, Germany) at 10,000 rpm for 10 min on ice. Next, the extract was treated with a
273 Q500 sonicator using a CL-334 converter (QSonica, Newtown, USA) at amplitude 55%, 10s on & 40s off
274 for 20 min at 8 °C. Debris was removed by two centrifugations at 4500 x g for 10 min and 20,000 x g for
275 20 min, both at 4 °C. The sample was combined with solid $(NH_4)_2SO_4$ to a final concentration of 45% (w/v)
276 and proteins precipitated under stirring for 1 h at 8 °C. Amounts of $(NH_4)_2SO_4$ were calculated using an
277 online tool (https://files.encorbio.com/protocols/AM-SO4.htm) (EnCor Biotechnology Inc., Gainesville,
278 USA). Precipitated proteins were pelleted by centrifugation at 12,000 x g for 10 min at 8 °C. Pellets were
279 dissolved in 4 mL cation exchange (CaEx) chromatography binding buffer (2.7 mM KCl, 10 mM Na_2HPO_4,
280 1.8 mM KH_2PO_4, 0.068 M NaCl, 0.01% (v/v) Tween 20, 5% (v/v) Glycerol, 5 mM DTT, pH 6.8) and dialyzed
281 (20k MW cut off, 88405, Thermo Fisher Scientific) overnight against the same buffer at 8 °C. The sample
282 was diluted to a final volume of 10 mL using binding buffer, and passed through a 0.22 µm filter (Roth,
283 Karlsruhe, Germany) before loading onto a 1 mL HiTrap SP HP cation exchange column (Cytiva,
284 Marlborough, USA), connected to an ÄKTA™ start (Cytiva). The column was washed with 5 column
285 volumes (CV) of 0.3 M NaCl (based on binding and elution buffer) and L1 eluted *via* 4 CV of elution buffer
286 (2.7 mM KCl, 10 mM Na_2HPO_4, 1.8 mM KH_2PO_4, 1 M NaCl, 0.01% (v/v) Tween 20, 5% (v/v) Glycerol, 5 mM
287 DTT, pH 6.8)

288 Eluted fractions containing L1 were pooled and dialyzed against disassembly buffer (22.7 mM KCl,
289 10 mM Na_2HPO_4, 1.8 mM KH_2PO_4, 0.068 M NaCl, 0.05% (v/v) Tween20, 5 mM DTT, pH 8.5) overnight at 8
290 °C with 3x buffer exchange. Samples were concentrated 5x using a vacuum concentrator (Concentrator
291 plus, Eppendorf, Hamburg, Germany). For reassembly, samples were dialyzed against reassembly buffer
292 (22.7 mM KCl, 10 mM Na_2HPO_4, 1.8 mM KH_2PO_4, 1 M NaCl, 0.05% (v/v) Tween20, pH 6) overnight at 8 °C
293 with 3x buffer exchange.
294

295 **SDS-PAGE and western blot**

296 SDS-PAGE and western blots were performed based on Bohlender et al. (2022). Two systems were
297 used for protein separation, either 7.5% polyacrylamide gels (Mini-PROTEAN® TGX™ Precast Gels, Rio-
298 Rad, Munich, Germany) in TGS buffer at 120 V, or 4 – 12% Bis-Tris gels (mPAGE™ Precast Gels, Merck,
299 Darmstadt, Germany) in MOPS buffer at 150 V. As first antibody served 1:5000 diluted CamVir1 (Thermo
300 Fisher Scientific), as second antibody peroxidase-linked rabbit anti-mouse secondary antibody (Cytiva)
301 diluted 1:12,500. For dot blots, protein samples were blotted on a PVDF membrane (Cytiva) using a
302 filtration manifold kit (SRC-96/1, Schleicher&Schuell, Dassel, Germany). Antibody H16.V5
303 (AntibodySystems, Schiltigheim, France) was diluted 1:5000. Dot blots were developed as described for
304 western blots. Yeast-produced HPV-16 L1 (Abcam, Cambridge, UK) was used as a positive control.
305

306 **L1 quantification**

307 The ELISA protocol was based on Studentsov et al. (2002). In short, 96-well microtiter plates
308 (Greiner, Kremsmünster, Austria) were coated with 1:500 CamVir1 antibody (Thermo Fisher Scientific) in
309 PBS overnight at 8 °C. Wells were washed twice with washing buffer (1x PBS, 0.05% (v/v) Tween20) and
310 blocked with blocking buffer (1x PBS, 1% (w/v) polyvinyl alcohol MW 47,000, 0.05% (v/v) Tween20) for 3
311 h at 37 °C. After 3x washing, samples were diluted in blocking buffer and incubated in the wells for 1.5 h
312 at 37 °C. Wells were washed 3x before adding 1:1000 diluted polyclonal anti-HPV-16 L1 antibody from
313 rabbit (Cusabio, Houston, USA) for 1 h at 37 °C. After 5x washing, wells were incubated with 1:1000 diluted
314 anti-rabbit HRP-conjugated antibody NA934 (Cytiva) for 1 h at 37°C. Wells were washed 3x before adding
315 100 µL TMB substrate (Thermo Fisher Scientific). The reaction was stopped with 50 µL of 2 M H_2SO_4.
316 Absorbance was measured at 450 / 595 nm for reference. The signal of a wildtype sample was subtracted
317 to account for background signal.
318

319 **Transmission electron microscopy**

320 The TEM protocol was based on Abel et al. (1989). Negative staining of purified VLPs and moss
321 extracts was performed using 300 Mesh glow discharged formvar/carbon-coated copper grids (Electron
322 Microscopy Sciences, Hatfield, USA). Five µL of sample were applied on a grid and incubated for 5 min at
323 RT. Grids were washed 3x with water and stained with 2% (w/v) uranyl acetate. After 30 sec, uranyl
324 acetate was removed with a filter paper, grids were air dried, and inspected with a Hitachi HT7800 TEM
325 (Tokyo, Japan) coupled to a Xarosa CMOS camera (Emsis, Münster, Germany).
326

327 ## Results

328 **Adaptation of L1 coding sequence for Physcomitrella-optimized expression**

329 The coding sequence (CDS) of HPV-16 L1 was optimized for expression in Physcomitrella. The goal
330 was to adapt the CDS regarding codon usage and preventing potential degradation through microRNAs
331 and splicing. A human codon-optimized version (hL1, **Supplementary Figure S2**) was used as a basis for
332 optimization since it had led to higher yields than plant-optimized versions or the native viral sequence in
333 *Nicotiana benthamiana* (Maclean et al., 2007).
334 For codon optimization, physCO (Top et al., 2021) was used, which changed nine out of 505
335 codons and slightly increased the GC content from 62.25% to 62.85% (**Supplementary Figure S2**). Next,
336 the CDS was scanned for the motif AGGT, which is the most common motif at exon-intron borders for
337 alternative splicing in Physcomitrella (Top et al., 2021). Transformation of a heterologous cDNA containing
338 the AGGT motif led to alternative splicing in Physcomitrella, a process referred to as heterosplicing (Top
339 et al., 2021). Scanning the physCO-optimized hL1 sequence yielded 5 AGGT-motifs which were replaced
340 by synonymous codons (**Supplementary Figure S2**). MicroRNAs bind complementary sequences in the
341 mRNA and thereby cause inhibition of translation or degradation of mRNA (Jones-Rhoades et al., 2006;
342 Khraiwesh et al., 2010). One microRNA binding site was predicted within the CDS using psRNATarget (Dai
343 and Zhao, 2011; Dai et al., 2018). Therefore, we changed three bases within the predicted binding region
344 using synonymous codon substitutions. The final Physcomitrella-optimized CDS was named pL1
345 (**Supplementary Figure S2**) and differs from hL1 by 17 out of 1515 nucleotides without changing the amino
346 acid (aa) sequence.
347
348

349 **Characterization of chloroplast transit peptides**

350 Different constructs were designed to target L1 to specific cellular compartments, including
351 chloroplasts. Fusing chloroplast transit peptides (CTPs) to the L1 CDS led to increased protein yields in
352 tobacco as compared to constructs lacking CTPs (Maclean et al., 2007; Zahin et al., 2016). To assess
353 whether this is also true for L1 production in Physcomitrella, a selection of Physcomitrella-derived CTPs
354 was characterized.

355 Initially, the CTP of FtsZ1-1 (Gremillon et al., 2007) was considered. However, cleavage site
356 analysis *via* TargetP-2.0 (Armenteros et al., 2019) predicted 37 aa of this CTP to remain at the N-terminus
357 of L1 after chloroplast import. This CTP was rejected because the additional aa could change L1 properties
358 and hamper VLP assembly. A list of alternative CTPs was derived from the Physcomitrella N-terminome
359 (Hoernstein et al., 2024) (**Supplementary Table S2**). Here, experimentally detected protein N-termini
360 were compared with TargetP-2.0 predictions for cleavable N-terminal targeting sequences. Five CTPs were
361 selected where an exact match between prediction and experimentally validated N-terminus was
362 observed across different experiments (Hoernstein al., 2024), namely CTPc5, CTPc10.1, CTPc10.2, CTPc21,
363 CTPc22 (**Table 1**). Their sequences were fused *in silico* to the N-terminus of L1 and analyzed with TargetP-
364 2.0 to validate the correct cleavage of the fusion.

365 Our *in-silico* analysis indicated CTPc22 to end with a methionine, which could introduce an
366 alternative translation initiation site, resulting in translation of L1 without the CTP (**Table 1**). Therefore,
367 an alternative version lacking the C-terminal methionine (CTPc22noMet) was included. The likelihoods for
368 chloroplast localization were above 70% for all candidates except CTPc10.1 (**Table 1**), which was rejected.

369 The remaining five CTPs (CTPc5, CTPc10.2, CTPc21, CTPc22, CTPc22noMet) were fused to the CDS
370 of eGFP (**Supplementary Figure S1**) and expressed in Physcomitrella protoplasts. Analysis *via* fluorescence
371 microscopy confirmed localization of eGFP signals in chloroplasts for CTPc5, CTPc10.2, CTPc22, and
372 CTPc22noMet, but not for CTPc21 (**Supplementary Figure S3**). Of the four remaining CTPs, CTPc5 had the
373 highest likelihood for plastid localization (**Table 1**) and were examined *via* confocal microscopy
374 (**Supplementary Figure S3**). Finally, we selected CTPc5 for the chloroplast-targeting of L1.
375

376 **Table 1. *In-silico* analysis of Physcomitrella-derived chloroplast transit peptides.** CTPs were selected
377 based on mass spectrometry datasets (Hoernstein et al., 2024). *In-silico* predictions of likelihood of
378 chloroplast localization target sequence cleavage were performed with TargetP-2.0.

Name of CTP	Originating from protein model	Predicted cleavage of CTP-L1	Length (aa)	Likelihood of GFP chloroplast localization	Likelihood of L1 chloroplast localization
FtsZ1-1	Pp3c22_4940V3.1	37 aa remain on N-terminus	84	0.95	0.92
CTPc5	Pp3c5_1370V3.1	-	74	0.987	0.943
CTPc10.1	Pp3c10_10490V3.1	-	63	0.456	0.229
CTPc10.2	Pp3c10_2940V3.1	-	70	0.908	0.845
CTPc21	Pp3c21_9980V3.1	-	43	0.956	0.891
CTPc22	Pp3c22_5470V3.1	-	62	0.939	0.739
CTPc22noMet	Pp3c22_5470V3.1	-	61	0.913	0.727

379

380 **Targeting of L1 to nuclei and chloroplasts**

381 To evaluate the impact of L1 localization on product yield, we generated three variants (pL1,
382 pL1Δ22, CTP-pL1). pL1 contains the full-length pL1 CDS, which includes the native HPV-16 NLS (Cerqueira
383 and Schiller, 2017). For pL1Δ22 the NLS was removed. In CTP-pL1 the Physcomitrella CTPc5 was fused to
384 the 5' of the pL1 CDS, including the NLS.

385 After generation of these CDS variants, we aimed to evaluate L1 targeting to subcellular
386 compartments. The CDS of pL1, pL1Δ22 and CTP-pL1 were fused to the 5' end of Citrine CDS
387 (**Supplementary Figure S1**). Physcomitrella protoplasts were transfected with the plasmids and Citrine
388 localization was analyzed using fluorescence microscopy. A vector encoding Citrine without any L1 variant
389 fusion served as a control.

390 Cells transformed with the control vector exhibited predominantly cytoplasmic Citrine signals,
391 whereas diffuse signals also occurred in nuclei (**Figure 1**). For pL1-Citrine, the signal localized to nuclei,
392 demonstrating that the HPV-16 NLS is functional in Physcomitrella. This is further supported by the fact
393 that removal of the NLS in pL1Δ22-Citrine results in cytoplasmic localization of the signal. For CTP-pL1-

394 Citrine, the signal is predominantly in chloroplasts, but is not evenly distributed, as seen for CTP-eGFP
395 fusions lacking L1 (**Supplementary Figure S3**). Instead, the pL1-Citrine fusion concentrates in several spots
396 of high fluorescence intensity and less than 1 µm in diameter. It is unclear whether this difference is due
397 to distinct features of GFP and Citrine or due to the presence of L1 and potential formation of L1
398 multimeric structures. Overall, we confirmed successful L1 targeting to the intended compartments.
399

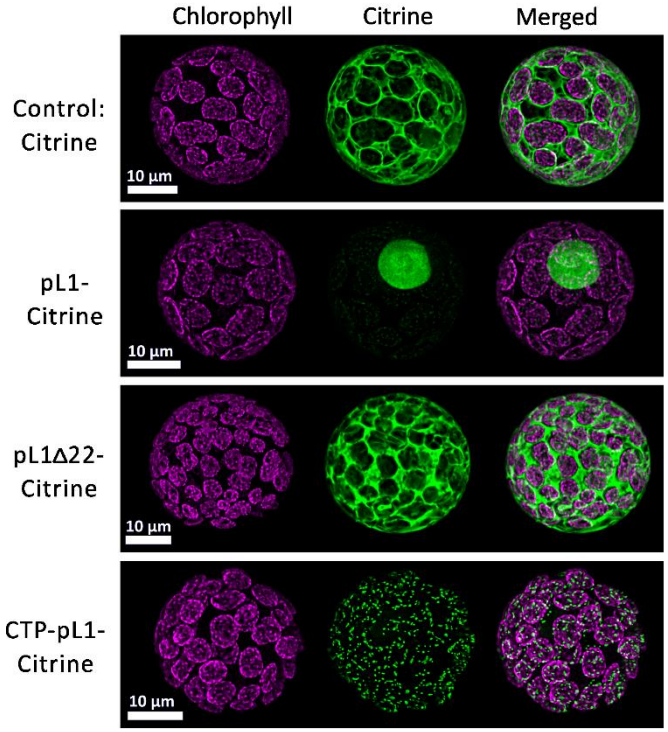

400
401

402 **Figure 1. Subcellular localization of L1 variants.** Confocal microscopy images of Physcomitrella
403 protoplasts transformed with constructs encoding (CTP-)pL1(Δ22)-Citrine fusion proteins or Citrine alone.
404 For each sample, chlorophyll autofluorescence in magenta is seen on the left, Citrine signals in the middle
405 and the merged signals on the right. In the control and pL1Δ22-Citrine, the Citrine signals do not enter the
406 chloroplasts and are mainly in the cytoplasm. For pL1-Citrine, the Citrine signals are in the nucleus. In the
407 CTP-pL1-Citrine sample, the Citrine signals form small spots of high intensity in the chloroplasts.
408

409 **Characterization of L1 production**

410 After validating the subcellular localization, pL1, pL1Δ22 and CTP-pL1 expression constructs were
411 cloned (**Supplementary Figure S1**). The linearized constructs were transferred into Physcomitrella
412 protoplasts and obtained plants were screened for productivity by western blot and ELISA.

413 Western blot analysis revealed the L1 monomer of 56 kDa (pL1, CTP-pL1) and 54 kDa (pL1Δ22)
414 (**Figure 2**). In addition, pL1 and CTP-pL1 lines exhibited a band at approximately 54 kDa. All lines showed
415 another band at around 45 kDa, even though the signal was relatively weak in CTP lines and more
416 prominent in pL1Δ22 lines. Smaller protein isoforms can originate from degradation or DNA or RNA,
417 resulting in truncated transcripts and, subsequently, truncated protein isoforms (Murén et al., 2009; Top
418 et al., 2021). The latter possibilities were ruled out by amplifying the L1 CDS *via* PCR from cDNA, which
419 yielded amplicons of the expected sizes, corresponding to the western blot bands of 56 kDa (pL1, CTP-
420 pL1) and 54 kDa (pL1Δ22), but not additional amplicons (**Supplementary Figure S4**). Also, two bands are
421 visible at 130 – 180 kDa, of which the highest band at 180 kDa is also present in the yeast-produced L1
422 control. This pattern of two close-by bands repeats another two times at higher molecular weight outside
423 of the marker range (**Figure 2**). Addition of reducing agents DTT or ascorbic acid to the extraction buffer
424 markedly reduces the western blot signal intensity above 180 kDa (**Supplementary Figure S5**). We
425 hypothesize that in the absence of reducing agents, reactive oxygen species (ROS) in the plant extract
426 cross-link L1 with itself and/or host proteins. Irrespective of the presence or absence of reducing agents
427 during extraction and purification, two prominent bands in the range of 130 and 180 kDa are present in
428 all western blots (**Figures 2 and 4, Supplementary Figure S7**). Western blot and ELISA analysis indicate
429 higher yields in CTP-pL1 lines as compared to pL1 or pL1∆22 lines. In shaking flasks, the best producer is
430 CTP-pL1 30 with 142 µg L1/g FW (**Figure 2**).
431 Besides the amount of recombinant protein per g FW biomass, the accumulation of biomass is
432 important in biomanufacturing as high product yields per biomass can be trivial if biomass accumulation
433 is slow. To study if recombinant protein amount or subcellular localization of L1 hampers plant growth,
434 we analyzed the time course of biomass accumulation of the nine lines in shaking flasks for 4 weeks.
435 In our conditions, exponential growth could not be measured. This might be due to the culture
436 conditions, to the rather long intervals between sampling, and/or to the intrinsic growth characteristics
437 of Physcomitrella protonema, which grows by apical cell division (Reski, 1998). Therefore, biomass density
438 was fitted using linear regression analysis model (**Supplementary Figure S6**), using the calculated slope to
439 approximate biomass accumulation rates. Comparison of the slopes between the lines pL1, pL1Δ22 and
440 CTP-pL1 showed pL1 lines accumulated biomass faster than pL1Δ22 ($p = <0.0001$) and CTP-pL1 ($p = 0.0001$)
441 lines. If this difference is due to the distinct L1 localization or to lower L1 production in pL1 lines (**Figure**
442 **2**) is unclear. Line pL1 47B showed the highest slope of 255 mg dry weight (DW)/L/week, as compared to
443 line CTP-pL1 30 with a slope of 211 mg DW/L/week. However, this difference is negligible considering the

yield of pL1 47B is 8 µg L1/g FW as to 142 µg L1/g FW for CTP-pL1 30 (**Figure 2**). Consequently, line CTP-pL1 30 was chosen for VLP production.

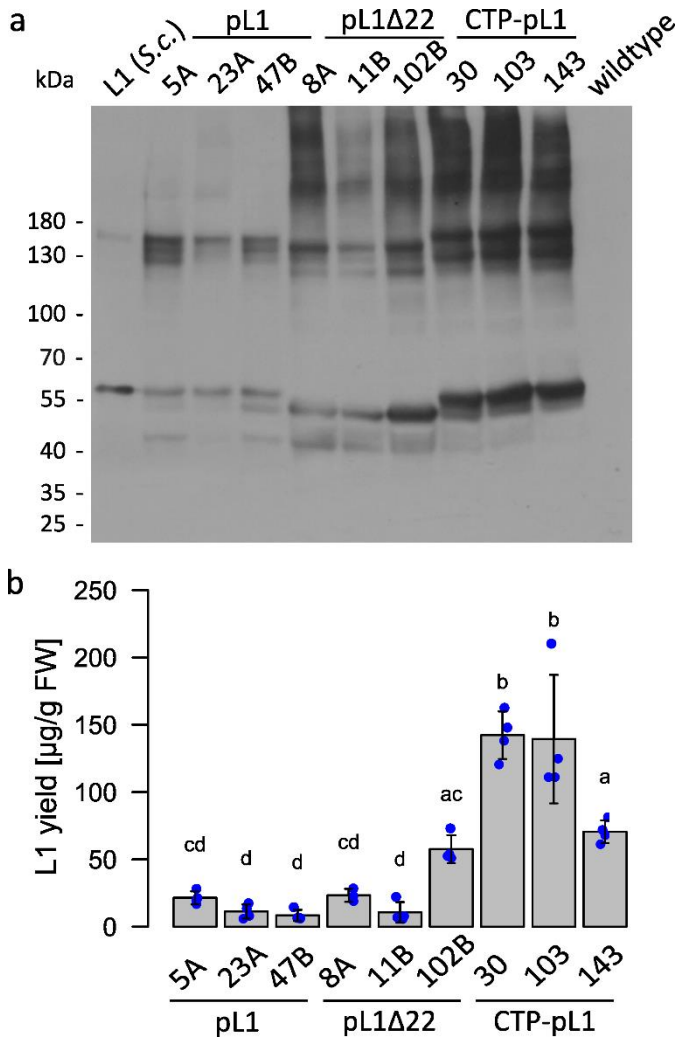

Figure 2: Analysis of HPV-16 L1 production *via* western blot and ELISA. (**a**) For each of the constructs pL1, pL1Δ22, and CTP-pL1 three lines were tested *via* western blot for expression of HPV-16 L1. 50 ng *S. cerevisiae*-produced L1 served as a positive control and Physcomitrella wildtype as a negative control. The proteins for the western blot were separated on a 7.5% TGS polyacrylamide gel under reducing conditions before being transferred to a membrane and developed using CamVir1 antibody (1:5000). (**b**) Production levels of L1 were quantified *via* ELISA. Wildtype background signal was subtracted before analysis *via* one-way ANOVA and post hoc multiple comparisons test (TukeyHSD). Means and standard deviations are calculated based on n ≥ 3 technical replicates from two dilutions and are given per biomass fresh weight (FW). Statistical significance (α = 0.05) is indicated by Compact Letter Display.

458

459 **Upscaled L1 production**

460 For production of VLPs, the cultivation of line CTP-pL1 30 was upscaled to 5 L-photobioreactors.
461 The goal here was to identify the best time point for harvesting material used for subsequent L1
462 purification.

463 Biomass increased from initially 60 mg DW/L to around 870 mg DW/L at day 4 (**Figure 3**). L1
464 production remained constant during the first 4 days, in the range of the yield observed for flasks. Upon
465 addition of the phytohormone auxin (NAA) on day 4, L1 levels increased on day 6 and peaked at day 7 at
466 332 µg/g FW, 130% higher as compared to day 0. Afterwards, L1 production dropped sharply to levels
467 prior to auxin addition. Biomass continued to accumulate until day 11, after which it dropped slightly.
468 These conditions, including day 7 as the ideal harvesting time point, were used for further L1 production.

469

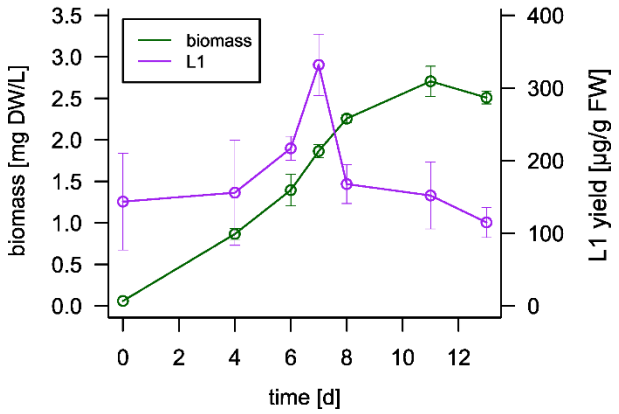

470
471

472 **Figure 3. Analysis of biomass accumulation and L1 production of line CTP-pL1 30 in a 5 L-**
473 **photobioreactor.** The bioreactor was inoculated with 60 mg dry weight (DW)/L and monitored over a
474 course of 13 days. On day 4, 5 µM auxin (NAA) was added. L1 production peaked at day 7 at 332 µg/g
475 fresh weight (FW). Biomass and L1 measurements are based on n ≥ 3 technical replicates. Production
476 levels of L1 were quantified *via* ELISA.

477

478 **Two-step purification removes bulk of cellular proteins**

479 Purification of L1 was performed using ammonium-sulfate (AMS) precipitation, followed by cation
480 exchange (CaEx) chromatography. While AMS removes the bulk of cellular proteins, CaEx removes
481 residual proteins and concentrates the sample.

482 We tested the efficacy of 40%, 45% and 50% (w/v) AMS to precipitate L1 from an extract
483 containing the soluble protein fraction from CTP-pL1 30 plant material produced in the bioreactor. We
484 found 45% AMS to be sufficient to effectively remove L1 from the supernatant, whereas at 40% AMS small
485 amounts of L1 remained in the supernatant and at 50% AMS higher amounts of cellular protein were
486 precipitated together with L1 (**Supplementary Figure S7**). In preparation for chromatographic purification,
487 the precipitated proteins were resuspended in CaEx binding buffer and dialyzed overnight in binding
488 buffer to remove residual AMS. Cloudiness of samples indicated a reduced solubility of precipitated
489 proteins, and undissolved matter was removed by filtration. The relative amount of L1 and host protein
490 was evaluated *via* western blots and Coomassie-staining, respectively (**Supplementary Figure S7**).
491 Samples after filtration showed a slight reduction in host protein content, but, except for the sample at
492 40% AMS, no reduction in L1. Overall, precipitation at 45% AMS was selected, which is in line with
493 purifications of yeast-produced L1 (Park et al., 2008; Kim et al., 2010).
494 Next, CaEx chromatography was used to remove residual cellular proteins. The bulk of cellular
495 proteins did not bind to the column and was detected in the flow through (**Figure 4**, **Supplementary Figure**
496 **S8**). Notably, a large amount of L1 did not bind to the column and was detected in the flow through.
497 Different binding buffer compositions were tested to increase L1 binding to the column, e.g. lowering the
498 pH from 7.2 to 6.8, lowering the concentration of NaCl from 0.137 M to 0.068 M, addition of 5% (v/v)
499 glycerol, and re-loading of flow-through fraction. Nevertheless, a large part of L1 did not bind to the
500 column and was found in the flow through. During column wash with 5 mL at 0.3 M NaCl, small amounts
501 of contaminating proteins and L1 were washed off the column. For elution, NaCl was increased to 1 M
502 NaCl and 0.5 mL fractions were collected, in total 4 mL. L1 eluted from the column in fractions E4 – E8
503 (**Figure 4**), which were pooled for further analysis.
504
505

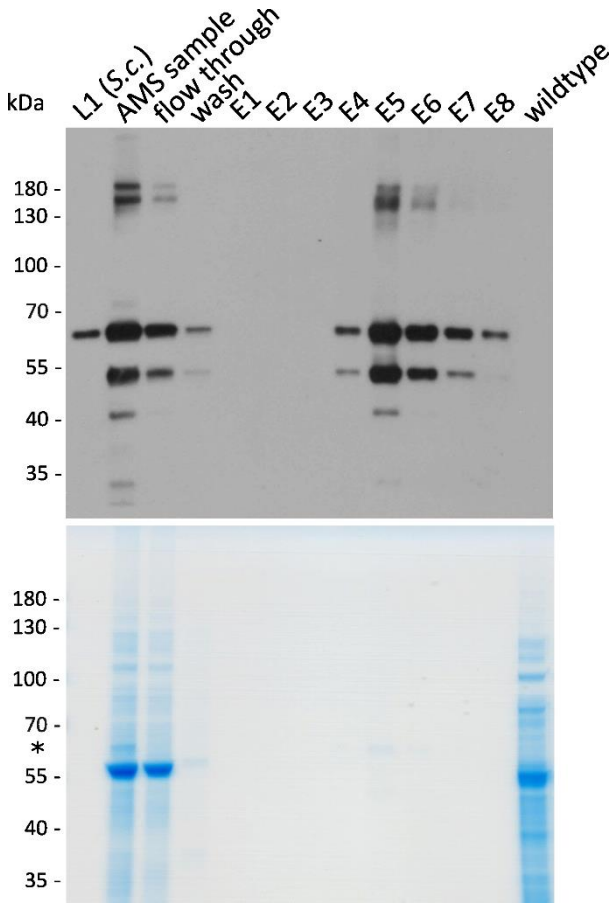

Figure 4. Two-step purification of L1 removes bulk of cellular protein. Analysis of L1 and residual cellular host proteins during purification under reducing conditions *via* western blot and Coomassie-stained SDS-PAGE (12% Bis-Tris gel). After precipitation with 45% (w/v) AMS, the filtered sample was subjected to cation exchange chromatography (CaEx) for final purification. Column-bound L1 eluted at 1 M NaCl in fractions E4 – E8. The asterisk in the Coomassie-stained SDS-PAGE marks the band referring to HPV-16 L1. 50 ng *S. cerevisiae*-produced L1 served as a positive control and Physcomitrella wildtype as a negative control.

Capsomers and VLPs

Next, we performed a dis- and reassembly protocol on the pooled elution fractions, as it yields more uniform and stable VLPs, which are less prone to aggregation (McCarthy et al., 1998; Mach et al., 2006). First, pooled elution fractions were dialyzed at low salt concentrations, high pH and DTT, that results in the disassembly of VLPs or other multi-pentameric L1-based structures into capsomers. Second,

521 samples were dialyzed at high salt, low pH and in the absence of reducing agent, that leads to the
522 reassembly of capsomers into VLPs.

523 To assess the conformation of L1 throughout the process, dot blots were performed using
524 different monoclonal antibodies. CamVir1 detects a linear epitope in both denatured and native L1 and
525 served as a control. In contrast, H16.V5 detects only conformational epitopes in both, L1 capsomers and
526 VLPs, but not monomeric or denatured L1.

527 The dot blot showed the presence of L1 in all CTP-pL1 30-derived samples throughout the
528 purification process, as well as yeast-derived denatured and native L1 (**Figure 5**). In comparison, H16.V5
529 detects L1 in the native positive control and in all CTP-pL1 30-derived samples, indicating the presence of
530 at least capsomers, if not VLPs, already in the raw extract. Further, conformational epitopes seem to be
531 stable throughout AMS precipitation, CaEx chromatography, disassembly, and reassembly. However, the
532 reassembly sample exhibits a weaker signal for H16.V5 as compared to CamVir1.

533

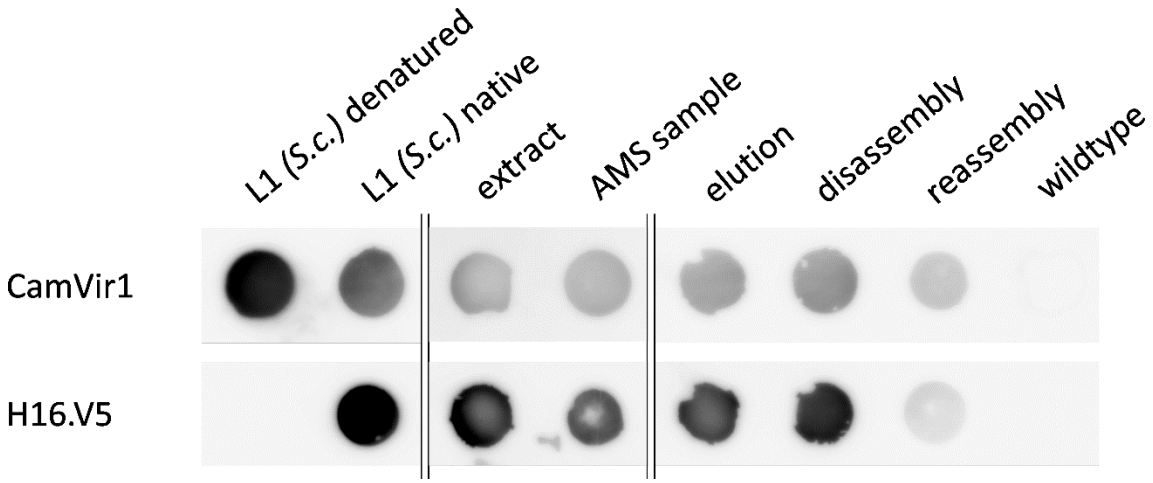

534
535

536 **Figure 5. Moss-produced HPV-16 L1 assembles into capsomers, which are stable throughout**
537 **purification.** Dot blots were performed using two different antibodies to analyze the formation of
538 capsomers in yeast-produced L1 and samples from CTP-pL1 30 purification (extract, after AMS
539 precipitation, elution) and dis- and reassembly. The CamVir1 antibody detects a linear epitope in both
540 denatured and native L1. The neutralizing antibody H16.V5 detects specifically conformational epitopes
541 in L1 capsomers and VLPs. Positive H16.V5 signals indicate HPV-16 L1 monomers to assemble at least into
542 capsomers, *in vivo* or after extraction, which are stable throughout the purification. The experiment only
543 allows qualitative but not quantitative comparison since sample concentrations were adjusted

individually. `L1 denatured´ was incubated at 95 °C for 5 min, all other samples were kept at 4 °C. A wildtype sample was used as a negative control.

The assembly of L1 into VLPs was verified with Transmission Electron Microscopy (TEM). As a control, yeast-produced L1 was analyzed without prior treatment, after disassembly, and after reassembly. In the untreated sample, particles of approx. 60 nm in size were detected. After disassembly, structures of 5 – 10 nm in size were observed, corresponding in size and appearance to capsomers observed for yeast-derived L1 as part of this study (**Figure 6b**) and elsewhere (McCarthy et al., 1996). VLPs reshape upon reassembly treatment, demonstrating the successful dis- and reassembly of yeast-derived L1 VLPs. Notably, reassembled VLPs are heterogenous in size and shape, despite the controlled dis- and reassembly (**Figure 6**).

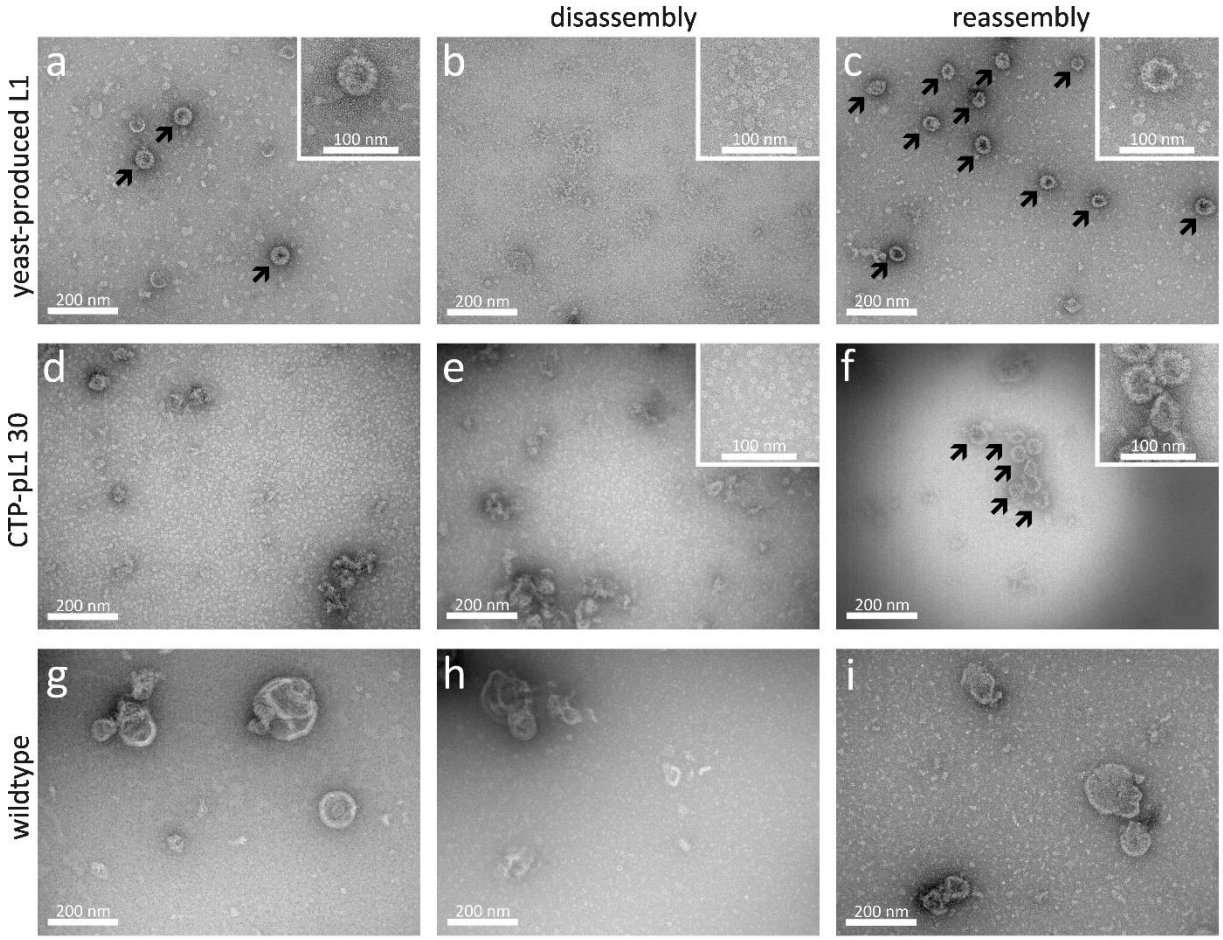

558 **Figure 6. Analysis of dis- and reassembled VLPs from moss and yeast *via* transmission electron**
559 **microscopy (TEM).** Yeast-derived L1 was analyzed untreated (**a**), after disassembly (**b**), and after
560 reassembly (**c**) *via* TEM. CTP-pL130 (**d** – **f**) and wildtype (**g** – **i**) extracts were purified *via* AMS precipitation
561 and CaEx chromatography (**d** & **g**), after disassembly (**e** & **h**), and after reassembly (**f** & **i**). Untreated yeast-
562 derived VLPs (**a**) disintegrate into capsomers upon disassembly (**b**) and reshape into VLPs upon reassembly
563 treatment (**c**). TEM shows the presence of moss-derived HPV-16 L1 capsomers in the elution (**d**) and
564 disassembly sample (**e**) and the assembly into VLPs in the reassembly sample (**f**). Capsomer and VLP-like
565 structures are absent from the wildtype control samples. VLPs are indicated by black arrows.
566
567 To analyze L1 assembly into VLPs, samples were taken from the pooled CaEx chromatography
568 elution fractions, after disassembly, and after reassembly.
569 In the elution sample, no VLPs but capsomeric structures were observed, comparable to those in
570 the disassembled yeast sample, which are not present in the corresponding wildtype control (**Figure 6**).
571 The abundance of capsomers in the elution fractions was surprising given the fact that the elution buffer
572 has a high ionic strength, which favors reassembly. However, before column loading, the sample was
573 dialyzed overnight in binding buffer, which favors disassembly. The exposure to high ionic strength during
574 elution might have been too short to allow VLP assembly. In addition, both binding and elution buffer
575 contained DTT, which induces disassembly (McCarthy et al., 1998; Mach et al., 2006). The disassembled
576 CTP-pL1 30-derived sample depicted capsomers as seen in the elution fraction, and for disassembled
577 yeast-derived L1 (**Figure 6**). **Figure 6f** displays fully assembled, moss-derived HPV-16 L1 VLPs. Again, VLPs
578 were heterogenous in size and shape, as seen for reassembled yeast-derived VLPs. Moss-produced VLPs
579 tended to aggregate, which was not observed for reassembled yeast-derived VLPs, but is common for
580 HPV-16 L1 VLPs (Shi et al., 2005). Aggregation might also explain the relatively low signal for the
581 conformational antibody H16.V5 in the sample of reassembled moss-derived VLPs (**Figure 5**). No VLPs
582 were detected in wildtype samples (**Figure 6**).
583

584 ## Discussion

585 The goal of this study was to gain proof-of-concept for the production of virus-like particles (VLPs)
586 in the moss plant Physcomitrella by producing HPV-16 L1 VLPs. For this purpose, we generated a coding
587 sequence (CDS) optimized for expression of HPV-16 L1 in Physcomitrella. We further characterized five
588 chloroplast transit peptides (CTPs) and confirmed the localization of L1 in chloroplasts. In addition, we

589 demonstrated chloroplast localization to yield higher L1 levels than targeting the protein to nuclei or
590 cytoplasm. Cultivation in photobioreactors yielded more than 0.3 mg / g FW, which is in the range of other
591 plant-based expression platforms. We established a purification protocol and demonstrated the
592 successful assembly of moss-produced HPV-16 L1 VLPs.

593 In tobacco plants (*Nicotiana benthamiana*), various strategies were explored for increasing
594 production yields of HPV-16 L1 VLPs, one of which is optimization of codon usage (Maclean et al., 2007;
595 Hitzeroth et al., 2018). Hitzeroth et al. (2008) found that codon optimization of L1 improves transcription,
596 rather than translation. This is due to RNA motifs in the L1 CDS, which post-transcriptionally regulate the
597 virus life cycle and lead to pre-mRNA degradation (Mori et al., 2006; Zhao and Schwartz, 2008). It is argued
598 that codon optimization removes those motifs, thereby increasing mRNA and protein levels, irrespective
599 of whether the CDS was optimized for expression in humans, tobacco (Hitzeroth et al., 2018) or
600 Physcomitrella (this study). Our Physcomitrella-optimized CDS has a GC content of 62.85% as compared
601 to hL1 with 62.25% (Maclean et al., 2007) and the wildtype sequence with 38.27% (Varsani et al., 2003).
602 Combined with the removal of microRNA binding sites and heterosplice sites we obtained the
603 Physcomitrella-optimized pL1 CDS. We argue that pL1 addresses the issues of L1 intrinsic degradation
604 motifs as well as Physcomitrella-specific posttranscriptional degradation.

605 Besides codon optimization, research focused on localization signals and transit peptides. The
606 most common strategy is sequestration to chloroplasts, either *via* nuclear transformation and
607 posttranslational import into chloroplasts (Maclean et al., 2007; Matic et al., 2011; Pineo et al., 2013;
608 Zahin et al., 2016; Hitzeroth et al., 2018; Naupu et al., 2020; Muthamilselvan et al., 2023) or *via*
609 transplastomic lines (Fernández-San Millán et al., 2008; Lenzi et al., 2008). Here, we experimentally
610 characterized five Physcomitrella CTPs, of which we used one (CTPc5) for sequestration of L1 to
611 chloroplasts. Employing the HPV-16 native NLS, L1 was targeted to nuclei, whereas the removal of the NLS
612 resulted in cytoplasmic L1. Earlier studies confirmed functionality of the NLS in mammalian cells (Leder et
613 al., 2001; Bissa et al., 2015). However, the NLS failed to localize L1 to nuclei in tobacco (Šmídková et al.,
614 2010). Our observation of the HPV-16 native NLS targeting L1 to nuclei in Physcomitrella is another
615 example for a conserved cross-kingdom functionality of localization signals between moss and mammals
616 (Gitzinger et al., 2009).

617 Western blots of L1-producing Physcomitrella lines showed a variety of bands, both smaller and
618 larger than the expected 56 kDa or 54 kDa. A comparable banding pattern was observed when expressing
619 L1 in tobacco chloroplasts (Fernández-San Millán et al., 2008). Likewise, yeast-produced L1 exhibited
620 bands with the size of L1 dimers and trimers (Kim et al., 2007; Kim et al., 2010). L1 dimers and trimers are

621 based on inter-capsomeric disulfide bridges which stabilize virions and VLPs (Sapp et al., 1998; Buck et al.,
622 2005; Buck et al., 2013). McCarthy et al. (1998) resolved L1 multimers with DTT. Likewise, Buck et al.
623 (2005) demonstrated absence and presence of L1 dimers and trimers in a comparison of reducing and
624 non-reducing SDS-PAGE and western blots, respectively. An investigation of cysteine 175 and cysteine 428
625 L1 mutants resulted in the absence of bands at 130 kDa and 180 kDa, thereby linking disulfide bridge-
626 based dimers and trimers to the observed bands (Buck et al., 2005). Surprisingly, reducing agents such as
627 DTT, ascorbic acid or β-mercaptoethanol did not result in the disappearance of these bands in our and
628 other studies (Kim et al., 2007; Fernández-San Millán et al., 2008; Kim et al., 2010). This indicates a
629 tolerance of L1 dimers and trimers to reducing agents or a different origin of multimerization observed at
630 130 kDa and 180 kDa. Castells-Graells and Lomonossoff (2021) observed multimerization of *Nudaurelia*
631 *capensis* omega virus α-peptide produced in tobacco, irrespective of DTT, but not when produced in insect
632 cells. These authors hypothesize that cross-linkage of α-peptide occurs during extraction and purification
633 and occurs in plant-based expression systems. Regarding the observed bands below 56 kDa, proteolytic
634 degradation was proposed in other studies observing the same phenomenon (Buck et al., 2005;
635 Fernández-San Millán et al., 2008). In tobacco, a shift from bands above 100 kDa in young leaves to more
636 prominent bands at 45 kDa and 20 kDa in older leaves indicated proteolytic degradation of L1 over time
637 (Fernández-San Millán et al., 2008). In our study, bands at 45 kDa are most prominent in pL1Δ22 lines with
638 cytoplasmic L1 and less prominent for plastidic L1. This might result from organelle-specific proteases
639 (Coates at al., 2022).

640 In Physcomitrella, combining the full-length L1 with a CTP significantly increases L1 yield as
641 compared to full length L1 or L1 without NLS, which is in line with findings in tobacco (Maclean et al.,
642 2007; Zahin et al., 2016). In our study, L1 yields above 0.3 mg / g FW were achieved in the photobioreactor.
643 In tobacco, yields of 0.1 – 1.2 mg / g FW (Maclean et al., 2007; Pineo et al., 2013; Zahin et al., 2016;
644 Hitzeroth et al., 2018) and up to 3 mg / g FW in transplastomic lines have been reported (Fernández-San
645 Millán et al., 2008). The success of targeting L1 to chloroplasts over localization to other organelles may
646 have several reasons. One is that plastid L1 may be protected from proteases absent in chloroplasts (van
647 Wijk, 2024). Besides, CTPs also act on the transcriptional level. Upon expression in tobacco, chimeric L1/L2
648 transcripts containing a CTP were more abundant than transcripts lacking a CTP, and consequently yielded
649 more protein (Hitzeroth et al., 2018). So far, it is unclear whether this difference is due to enhanced
650 transcription, increased mRNA half-life or changes in mRNA secondary structure.

651 For purification of L1 from Physcomitrella extracts, we employed a combination of AMS
652 precipitation and CaEx chromatography. We found 45% AMS to be sufficient to efficiently precipitate L1.

653 Studies from yeast (Park et al., 2008; Kim et al., 2010) and tobacco (Zahin et al., 2016) also used 45% AMS,
654 whereas sometimes 50% AMS was used (Kim et al., 2018). CaEx chromatography showed that a large part
655 of L1 does not bind to the column. Likewise, Zahin et al. (2016) reported tobacco-produced L1 to bind
656 poorly to CaEx columns. Kim et al. (2010) purified yeast-produced L1 by either CaEx or heparin
657 chromatography. CaEx chromatography showed unbound L1 in the flow through, as observed in our
658 study, whereas no L1 was found in the flow through employing heparin chromatography. Pineo et al.
659 (2013) produced L1/L2 chimaeras in tobacco and experienced loss of L1 and insufficient removal of
660 contaminating proteins using heparin chromatography. Heparin is a highly sulfated form of heparan
661 sulfate, a proteoglycan found on host cell surfaces and a requirement for HPV virion attachment and
662 infection (Knappe et al., 2007). However, a prerequisite for heparin binding is the assembly of L1 to
663 capsomers or VLPs (Rommel et al., 2005), meaning monomers and not properly folded L1 are lost. Overall,
664 chromatography yields for VLPs differ and are influenced by different factors, including the production
665 host, the used materials and buffers, and purification prior to chromatography, making it difficult to
666 compare purification strategies across publications. Here, we achieved to remove the bulk of cellular
667 proteins from moss extracts, but experienced a substantial loss of L1 in the flow through. To address this,
668 further optimization of purification might be achieved by combinations with other methods such as
669 heparin chromatography. Our dot blot analysis confirmed the presence of intact capsomers or VLPs in
670 extracts and after AMS precipitation, suggesting heparin chromatography as an option for the second step
671 in purification.

672 TEM analysis of purified and reassembled CTP-pL1 samples shows VLPs of approx. 60 nm in size.
673 These nanoparticles assembled from capsomers as a result of the reassembly treatment. The absence of
674 VLPs in the elution fractions does not necessarily indicate that dis- and reassembly treatment is a
675 prerequisite for VLP formation from moss-produced L1, but rather that the buffer conditions did not favor
676 assembly after elution. To the best of our knowledge, this is the first report of VLPs produced in a non-
677 vascular plant and of *in vitro* reassembly of HPV-16 L1 VLPs from capsomers produced in any plant system.
678 The VLPs are heterogenous in shape and size. The same is true for yeast-derived VLPs after reassembly,
679 whereas untreated VLPs were not heterogenous. This is surprising, since controlled dis- and reassembly
680 of VLPs can enhance stability and uniformity (McCarthy et al., 1998; Mach et al., 2006; Shi et al., 2007).
681 Besides high ionic strength and low pH buffer, inter-pentameric disulfide bridges positively influence VLP
682 stability and uniformity (Buck et al., 2005). This could be achieved through prolonged incubation of cleared
683 cell lysates before purification or addition of oxidizing agents, which accelerate disulfide bridge formation.

684 However, prolonged incubation causes aggregation of HPV-16 L1 VLPs, as observed here, but could be
685 addressed by improved formulation (Shi et al., 2005).
686 While the moss plant Physcomitrella is an established production host for biopharmaceuticals, we
687 aim to expand its application to other markets such as the cosmetics industry (Munoz et al., 2024) and
688 material sciences at the interface with biomedicine (Milferstaedt et al., 2025; Ramezaniaghdam et al.,
689 2025). In this context, the present study serves as a proof-of-concept for the production of a relatively
690 simple but medicinally relevant VLP in Physcomitrella. Future efforts may focus on more complex eVLPs
691 that require proper N-glycosylation or complex folding and assembly; a specialty niche well suited for the
692 moss-based expression platform.
693
694
695

696 Acknowledgements

697 We thank the Life Imaging Centre (LIC) of the University of Freiburg for support with confocal microscopy.
698 We are grateful for technical assistance by Agnes Novakovic, Britta Rothgänger, Christine Glockner and
699 Richard Haas and to Anne Katrin Prowse for language editing.
700

701 Author contributions

702 PAN: Conceptualization, Formal analysis, Funding acquisition, Investigation, Methodology, Visualization,
703 Writing – original draft, Writing – review & editing
704 MCW: Investigation, Methodology, Writing – review & editing
705 SC: Investigation, Methodology, Writing – review & editing
706 CET: Investigation, Methodology, Formal analysis, Writing – review & editing
707 MRF: Investigation, Formal analysis, Writing – review & editing
708 SNWH: Investigation, Formal analysis, Writing – review & editing
709 JP: Writing – original draft, Writing – review & editing
710 ELD: Writing – original draft, Writing – review & editing
711 HTS: Conceptualization, Resources, Writing – review & editing
712 RR: Supervision, Resources, Writing – original draft, Writing – review & editing

Conflict of interest disclosure

RR is a founder of Greenovation Biotech, now Eleva Biologics, an inventor of the moss bioreactor, and currently serves as a member of Eleva's advisory board. HTS is a co-founder of Tailwind Biotech, a company designing DNA regulatory parts, and currently serves as a member of Tailwind's executive board. All other authors declare no conflict of interest.

Data availability statement

Nucleotide sequence data was submitted to GenBank under accession numbers PV029542 (pL1) and PV068547(CTPc5). Moss lines and vectors were submitted to the International Moss Stock Centre (IMSC) under accession numbers 40963 (pL1 5A), 40964 (pL1 23A), 40965 (pL1 47B), 40966 (pL1Δ22 8A), 40967 (pL1Δ22 11B), 40968 (pL1Δ22 102B), 40969 (CTP-pL1 30), 40970 (CTP-pL1 103), 40971 (CTP-pL1 143), 1840 (pAct5_linker_eGFP_35ST_hpt), 2038 (pAct5_CTP_linker_eGFP_35ST_hpt), 1193 (pAct5_Citrine_nosT_hpt), 2249 (pAct5_pL1-Citrine_nosT_hpt), 2250 (pAct5_pL1Δ22-Citrine_nosT_hpt), 2251 (pAct5_CTP-pL1-Citrine_nosT_hpt), 1997 (pAct5_pL1_35ST_hpt), 1998 (pAct5_pL1Δ22_35ST_hpt) and 2048 (pAct5_CTP-pL1_35ST_hpt).

Funding statement

This work was supported by Maria-Sklodowska-Curie Actions Innovative Training Network under the Horizon 2020 program under Grant Agreement No. 765115 (MossTech), by the German Research Foundation DFG under Germany's Excellence Strategy (CIBSS – EXC-2189 – Project ID 390939984), and the International Network Program by the Danish Agency for Higher Education and Science (grant number 1113-00016B). The TEM (Hitachi HT7800) was funded by a DFG grant (project number 426849454) and is operated by the University of Freiburg, Faculty of Biology, as a partner unit within the Microscopy and Image Analysis Platform MIAP and the Life Imaging Center LIC, Freiburg. PAN gratefully acknowledges financial support by Studienstiftung des deutschen Volkes.

740 ## Short legends for Supporting Information

741 Supplementary Figure S1 **Vector maps**

742 Supplementary Figure S2 **Generation of Physcomitrella-optimized (p)L1**

743 Supplementary Figure S3 **Characterization of CTPs by analysis of subcellular eGFP localization**

744 Supplementary Figure S4 **Analysis of CDS integrity in L1-producing lines**

745 Supplementary Figure S5 **Analysis of the effect of reducing agents on L1 band patterning**

746 Supplementary Figure S6 **Comparison of biomass accumulation rates**

747 Supplementary Figure S7 **Ammonium sulfate precipitation**

748 Supplementary Figure S8 **Chromatogram of Cation Exchange purification**

749 Supplementary Table S1 **List of primers**

750 Supplementary Table S2 **Predicted chloroplast transit peptides for six selected proteins in**

751 **Physcomitrella**

752 ## References

753 Abel WO, Knebel W, Koop HU, Marienfeld JR, Quader H, Reski R, Schnepf E, Sporlein B. A cytokinin-
754 sensitive mutant of the moss, *Physcomitrella patens*, defective in chloroplast division. Protoplasma (1989)
755 152:1-13. doi: 10.1007/BF01354234
756
757 Adams A, Hendrikse M, Rybicki EP, Hitzeroth II. Optimal size of DNA encapsidated by plant produced
758 human papillomavirus pseudovirions. Virology (2023) 580:88–97. doi: 10.1016/j.virol.2023.02.003
759
760 Armenteros JJA, Salvatore M, Emanuelsson O, Wither O, von Heijne G, Elofsson A, Nielsen H. Detecting
761 sequence signals in targeting peptides using deep learning. Life Sci All (2019) 2:e201900429. doi:
762 10.26508/lsa.201900429
763
764 Baker TS, Newcomb WW, Olson NH, Cowsert LM, Olson C, Brown JC. Structures of bovine and human
765 papillomaviruses. Analysis by cryoelectron microscopy and three-dimensional image reconstruction.
766 Biophys J (1991) 60:1445–1456. doi: 10.1016/S0006-3495(91)82181-6
767
768 Benvenuto E, Broer I, D'Aoust MA, Hitzeroth I, Hundleby P, Menassa R, Oksman-Caldentey KM, Peyret H,
769 Salgueiro S, Saxena P, Stander J, Warzecha H, Ma J. Plant molecular farming in the wake of the closure of
770 Medicago Inc. Nature Biotech (2023) 41:893–894. doi: 10.1038/s41587-023-01812-w
771
772 Biemelt S, Sonnewald U, Galmbacher P, Willmitzer L, Müller M. Production of human papillomavirus type
773 16 virus-like particles in transgenic plants. J Virol (2003) 77:9211–9220. doi: 10.1128/JVI.77.17.9211-
774 9220.2003
775
776 Bissa M, Zanotto C, Pacchioni S, Volonté L, Venuti A, Lembo D, De Giuli Morghen C, Radaelli A. The L1
777 protein of human papilloma virus 16 expressed by a fowlpox virus recombinant can assemble into virus-
778 like particles in mammalian cell lines but elicits a non-neutralising humoral response. Antiviral Res (2015)
779 116:67–75. doi: 10.1016/j.antiviral.2015.01.012
780

781 Bohlender LL, Parsons J, Hoernstein SNW, Rempfer C, Ruiz-Molina N, Lorenz T, Rodríguez Jahnke F, Figl R,
782 Fode B, Altmann F, Reski R, Decker EL. Stable protein sialylation in Physcomitrella. Front Plant Sci (2020)
783 11:610032. doi: 10.3389/FPLS.2020.610032
784
785 Bohlender LL, Parsons J, Hoernstein SNW, Bangert N, Rodriguez-Jahnke F, Reski R, Decker EL. Unexpected
786 arabinosylation after humanization of plant protein N-glycosylation. Front Bioeng Biotech (2022)
787 10:838365. https://doi.org/10.3389/fbioe.2022.838365
788
789 Buck CB, Thompson CD, Pang YYS, Lowy DR, Schiller JT. Maturation of papillomavirus capsids. J Virol (2005)
790 79:2839–2846. doi: 10.1128/JVI.79.5.2839-2846.2005
791
792 Buck CB, Day PM, Trus BL. The papillomavirus major capsid protein L1. Virol (2013) 445:169-174. doi:
793 10.1016/j.virol.2013.05.038
794
795 Burns CC, Diop OM, Sutter RW, Kew OM. Vaccine-derived polioviruses. J Infect Dis (2014) 210:S283-S293.
796 doi: 10.1093/INFDIS/JIU295
797
798 Büttner-Mainik A, Parsons J, Jérôme H, Hartmann A, Lamer S, Schaaf A, Schlosser A, Zipfel PF, Reski R,
799 Decker EL. Production of biologically active recombinant human factor H in Physcomitrella. Plant Biotech
800 J (2011) 9:373–383. doi: 10.1111/J.1467-7652.2010.00552.X
801
802 Castells-Graells R, Lomonossoff GP. Plant-based production can result in covalent cross-linking of proteins.
803 Plant Biotech J (2021) 19:1095–1097. doi: 10.1111/pbi.13598
804
805 Cerqueira C, Schiller JT. Papillomavirus assembly: An overview and perspectives. Virus Res (2017)
806 231:103–107. doi: 10.1016/j.virusres.2016.11.010
807
808 Chi H, Pepper M, Thomas PG. Principles and therapeutics of adaptive immunity. Cell (2024) 187:2052-
809 2078. doi: doi.org/10.1016/j.cell.2024.03.037
810
811 Coates RJ, Young MT, Scofield S. Optimising expression and extraction of recombinant proteins in plants.
812 Front Plant Sci (2022) 13:1074531. doi: 10.3389/fpls.2022.1074531

813

814 Cubas R, Zhang S, Li M, Chen C, Yao Q. Chimeric Trop2 virus-like particles: A potential immunotherapeutic
815 approach against pancreatic cancer. J Immunoth (2011) 34:251–263. doi: CJI.0B013E318209EE72
816

817 Dai X, Zhao PX. psRNATarget: a plant small RNA target analysis server. Nucl Acids Res (2011) 39:W155-
818 W159. doi: 10.1093/nar/gkr319
819

820 Dai X, Zhuang, Z, Zhao, PX. psRNATarget: a plant small RNA target analysis server (2017 release). Nucl
821 Acids Res (2018) 46:W49–W54. doi: 10.1093/NAR/GKY316
822

823 de Martel C, Georges D, Bray F, Ferlay J, Clifford GM. Global burden of cancer attributable to infections in
824 2018: a worldwide incidence analysis. Lancet Glob Health (2020) 8:e180–e190. doi: 10.1016/S2214-
825 109X(19)30488-7
826

827 Decker EL, Reski R. Mosses in biotechnology. Curr Op Biotech (2020) 61:21–27. doi:
828 10.1016/j.copbio.2019.09.021
829

830 Decker EL, Wiedemann G, Reski R. Gene targeting for precision glyco-engineering: Production of
831 biopharmaceuticals devoid of plant-typical glycosylation in moss bioreactors. Meth Mol Biol (2015)
832 1321:213-224. doi: 10.1007/978-1-4939-2760-9_15
833

834 Decker EL, Parsons J, Reski R. Glyco-engineering for biopharmaceutical production in moss bioreactors.
835 Front Plant Sci (2014) 5:346. doi: 10.3389/fpls.2014.00346
836

837 Eleva (2025). Eleva and 3PBIOVAN sign strategic GMP manufacturing and technology alliance to boost
838 capacity for Eleva's platform and pipeline. https://elevabiologics.com/eleva-and-3pbiovian-sign-
839 strategic-alliance [Accessed May 21, 2025].
840

841 Fernández-San Millán A, Ortigosa SM, Hervás-Stubbs S, Corral-Martínez P, Seguí-Simarro JM, Gaétan J,
842 Coursaget P, Veramendi J. Human papillomavirus L1 protein expressed in tobacco chloroplasts self-
843 assembles into virus-like particles that are highly immunogenic. Plant Biotech J (2008) 6:427–441. doi:
844 10.1111/j.1467-7652.2008.00338.x

845

846 Gibson DG, Young L, Chuang RY, Venter JC, Hutchison CA, Smith HO. Enzymatic assembly of DNA molecules
847 up to several hundred kilobases. Nature Met (2009) 6:343–345. doi: 10.1038/nmeth.1318
848

849 Gitzinger M, Parsons J, Reski R, Fussenegger M. Functional cross-kingdom conservation of mammalian and
850 moss (*Physcomitrella patens*) transcription, translation and secretion machineries. Plant Biotech J (2009)
851 7:73–86. doi: 10.1111/J.1467-7652.2008.00376.X
852

853 Gremillon L, Kiessling J, Hause B, Decker EL, Reski R, Sarnighausen E. Filamentous temperature-sensitive
854 Z (FtsZ) isoforms specifically interact in the chloroplasts and in the cytosol of *Physcomitrella patens*. New
855 Phyt (2007) 176:299–310. doi: 10.1111/j.1469-8137.2007.02169.x
856

857 Gupta R, Arora K, Roy SS, Joseph A, Rastogi R, Arora NM, Kundu PK. Platforms, advances, and technical
858 challenges in virus-like particles-based vaccines. Front Immun (2023) 14:1123805. doi:
859 10.3389/FIMMU.2023.1123805
860

861 Hasan SS, Sevvana M, Kuhn RJ, Rossmann MG. Structural biology of Zika virus and other flaviviruses. Nat
862 Struc Mol Biol (2018) 25:13–20. doi: 10.1038/s41594-017-0010-8
863

864 Hector M, Behnke V, Dabrowska-Schlepp, Busch A, Schaaf A, Langmann T, Wolf A. Moss-derived human
865 complement factor H modulates retinal immune response and attenuates retinal degeneration. J
866 Neuroinflam (2025) 22:104. doi: 10.1186/s12974-025-03418-2
867

868 Hennermann JB, Arash-Kaps L, Fekete G, Schaaf A, Busch A, Frischmuth T. Pharmacokinetics,
869 pharmacodynamics, and safety of moss-aGalactosidase A in patients with Fabry disease. J Inher Metab
870 Dis (2019) 42:527–533. doi: 10.1002/JIMD.12052
871

872 Hitzeroth II, Chabeda A, Whitehead MP, Graf M, Rybicki EP. Optimizing a human papillomavirus type 16
873 L1-based chimaeric gene for expression in plants. Front Bioeng Biotech (2018) 6:101. doi:
874 10.3389/fbioe.2018.00101
875

876 Hoernstein SNW, Oezdemir B, van Gessel N, Miniera AA, Rogalla von Bieberstein B, Nilges L, Schweikert
877 Farinha J, Komoll R, Glauz S, Weckerle T, Scherzinger F, Rodriguez-Franco M, Mueller-Schuessele S, Reski
878 R. A deeply conserved protease, acylamino acid-releasing enzyme (AARE), acts in ageing in Physcomitrella
879 and Arabidopsis. Comm Biol (2023) 6:61. doi: 10.1038/s42003-023-04428-7
880
881 Hoernstein SNW, Schlosser A, Fiedler K, van Gessel N, Igloi GL, Lang D, Reski R. A snapshot of the
882 Physcomitrella N-terminome reveals N-terminal methylation of organellar proteins. Plant Cell Rep (2024)
883 43:250. doi: 10.1007/s00299-024-03329-1
884
885 Hohe A, Reski R. Optimisation of a bioreactor culture of the moss *Physcomitrella patens* for mass
886 production of protoplasts. Plant Sci (2002) 163: 69-74. doi: 10.1016/S0168-9452(02)00059-6
887
888 Hohe A, Decker EL, Gorr G, Schween G, Reski R. Tight control of growth and cell differentiation in
889 photoautotrophically growing moss (*Physcomitrella patens*) bioreactor cultures. Plant Cell Rep (2002)
890 20:1135-1140. doi: 10.1007/s00299-002-0463-y
891
892 Hohe A, Egener T, Lucht JM, Holtorf H, Reinhard C, Schween G, Reski R. An improved and highly
893 standardized transformation procedure allows efficient production of single and multiple targeted gene-
894 knockouts in a moss, *Physcomitrella patens*. Curr Genet (2004) 44:339-347. doi: 10.1007/s00294-003-
895 0458-4
896
897 Jones-Rhoades MW, Bartel DP, Bartel B. MicroRNAs and their regulatory roles in plants. Ann Rev Plant
898 Biol (2006) 57:19-53. doi: 10.1146/annurev.arplant.57.032905.105218
899
900 Kerr H, Herbert AP, Makou E, Abramczyk D, Malik TH, Lomax-Browne H, Yang Y, Pappworth IY, Denton H,
901 Richards A, Marchbank KJ, Pickering MC, Barlow PN. Murine factor H co-produced in yeast with protein
902 disulfide isomerase ameliorated C3 dysregulation in factor H-deficient mice. Front Immun (2021)
903 12:681098. https://doi.org/10.3389/FIMMU.2021.681098
904
905 Khraiwesh B, Arif MA, Seumel GI, Ossowski S, Weigel D, Reski R, Frank W. Transcriptional control of gene
906 expression by microRNAs. Cell (2010) 140:111-122. doi: 10.1016/j.cell.2009.12.023
907

908 Kim SN, Jeong HS, Park SN, Kim HJ. Purification and immunogenicity study of human papillomavirus type
909 16 L1 protein in *Saccharomyces cerevisiae*. J Virol Met (2007) 139:24-30. doi:
910 10.1016/j.jviromet.2006.09.004
911
912 Kim HJ, Kim SY, Lim SJ, Kim JY, Lee SJ, Kim HJ. One-step chromatographic purification of human
913 papillomavirus type 16 L1 protein from *Saccharomyces cerevisiae*. Prot Expr Pur (2010) 70:68–74. doi:
914 10.1016/j.pep.2009.08.005
915
916 Kim HS, Jeon JH, Lee KJ, Ko K. N-glycosylation modification of plant-derived virus-like particles: An
917 application in vaccines. BioMed Res Int (2014) 2014:249519. doi: 10.1155/2014/249519
918
919 Kim HJ, Cho SY, Park MH, Kim HJ. Comparison of the size distributions and immunogenicity of human
920 papillomavirus type 16 L1 virus-like particles produced in insect and yeast cells. Arch Pharm Res (2018)
921 41:544–553. doi: 10.1007/s12272-018-1024-4
922
923 Kirnbauer R, Booy F, Cheng N, Lowy DR, Schiller JT. Papillomavirus L1 major capsid protein self-assembles
924 into virus-like particles that are highly immunogenic. Proc Nat Acad Sci USA (1992) 89:12180–84. doi:
925 10.1073/pnas.89.24.12180
926
927 Knappe M, Bodevin S, Selinka HC, Spillmann D, Streeck RE, Chen XS, Lindahl U, Sapp M. Surface-exposed
928 amino acid residues of HPV16 L1 protein mediating interaction with cell surface heparan sulfate. J Biol
929 Chem (2007) 282:27913–22. https://doi.org/10.1074/jbc.M705127200
930
931 Koprivova A, Stemmer C, Altmann F, Hoffmann A, Kopriva S, Gorr G, Reski R, Decker EL. Targeted
932 knockouts of *Physcomitrella* lacking plant-specific immunogenic N-glycans. Plant Biotech J (2004) 2:517–
933 523. doi: 10.1111/J.1467-7652.2004.00100.X
934
935 Lamprecht RL, Kennedy P, Huddy SM, Bethke S, Hendrikse M, Hitzeroth II, Rybicki EP. Production of human
936 papillomavirus pseudovirions in plants and their use in pseudovirion-based neutralisation assays in
937 mammalian cells. Sci Rep (2016) 6:20431. doi: 10.1038/srep20431
938

939 Leder C, Kleinschmidt JA, Wiethe C, Müller M. Enhancement of capsid gene expression: Preparing the
940 human papillomavirus type 16 major structural gene L1 for DNA vaccination purposes. J Virol (2001)
941 75:9201–09. doi: 10.1128/JVI.75.19.9201-9209.2001
942
943 Lenzi P, Scotti N, Alagna F, Tornesello ML, Pompa A, Vitale A, De Stradis A, Monti L, Grillo S, Buonaguro
944 FM, Maliga P, Cardi T. Translational fusion of chloroplast-expressed human papillomavirus type 16 L1
945 capsid protein enhances antigen accumulation in transplastomic tobacco. Transgen Res (2008) 17:1091–
946 1102. doi: 10.1007/s11248-008-9186-3
947
948 Lizotte PH, Wen AM, Sheen MR, Fields J, Rojanasopondist P, Steinmetz NF, Fiering S. *In situ* vaccination
949 with Cowpea Mosaic Virus nanoparticles suppresses metastatic cancer. Nat Nanotech (2015) 11:295–303.
950 doi: 10.1038/nnano.2015.292
951
952 Ljubojevic S, Skerlev M. HPV-associated diseases. Clin Derm (2014) 32:227-234. doi:
953 10.1016/j.clindermatol.2013.08.007
954
955 Lu B, Lim JM, Yu B, Song S, Neeli P, Sobhani N, K P, Bonam SR, Kurapati R, Zheng J, Chai D. The next-
956 generation DNA vaccine platforms and delivery systems: advances, challenges and prospects. Front
957 Immunol (2024) 15:1332939. doi: 10.3389/FIMMU.2024.1332939
958
959 Mach H, Volkin DB, Troutman RD, Wang B, Luo Z, Jansen KU, Shi L. Disassembly and reassembly of yeast-
960 derived recombinant human papillomavirus virus-like particles (HPV VLPs). J Pharm Sci (2006) 95:2195–
961 2206. doi: org/10.1002/jps.20696
962
963 Maclean J, Koekemoer M, Olivier AJ, Stewart D, Hitzeroth II, Rademacher T, Fischer R, Williamson AL,
964 Rybicki EP. Optimization of human papillomavirus type 16 (HPV-16) L1 expression in plants: comparison
965 of the suitability of different HPV-16 L1 gene variants and different cell-compartment localization. J Gen
966 Virol (2007) 88:1460–69. doi: org/10.1099/vir.0.82718-0
967
968 Marsian J, Lomonossoff GP. Molecular pharming – VLPs made in plants. Curr Op Biotech (2016) 37:201-
969 206. doi: 10.1016/j.copbio.2015.12.007
970

971 Matic S, Rinaldi R, Masenga V, Noris E. Efficient production of chimeric Human papillomavirus 16 L1
972 protein bearing the M2e influenza epitope in *Nicotiana benthamiana* plants. BMC Biotech (2011) 11:106.
973 doi: 10.1186/1472-6750-11-106
974
975 McCarthy MP, White WI, Palmer-Hill F, Koenig S, Suzich JA. Quantitative disassembly and reassembly of
976 human papillomavirus type 11 virus like particles *in vitro*. J Virol (1998) 72:32–41. doi:
977 10.1128/JVI.72.1.32-41.1998
978
979 Michelfelder S, Parsons J, Bohlender LL, Hoernstein SNW, Niederkrüger H, Busch A, Krieghoff N, Koch J,
980 Fode B, Schaaf A, Frischmuth T, Pohl M, Zipfel PF, Reski R, Decker EL, Häffner K. Moss-produced,
981 glycosylation-optimized human factor H for therapeutic application in complement disorders. J Am Soc
982 Nephrol (2017) 28:1462–74. doi: org/10.1681/ASN.2015070745
983
984 Michelfelder S, Fischer F, Wäldin A, Hörle KV, Pohl M, Parsons J, Reski R, Decker EL, Zipfel PF, Skerka C,
985 Häffner K. The MFHR1 fusion protein is a novel synthetic multitarget complement inhibitor with
986 therapeutic potential. J Am Soc Nephrol (2018) 29:1141–53. doi: 10.1681/ASN.2017070738
987
988 Milferstaedt SWL, Joest M, Bohlender LL, Hoernstein SNW, Özdemir B, Decker EL, van der Does C, Reski
989 R. Differential GTP-dependent in-vitro polymerization of recombinant Physcomitrella FtsZ proteins. Sci
990 Rep (2025) 15:3095. doi: 10.1038/s41598-024-85077-6
991
992 Mitsubishi Chemical Group Corporation. Overseas consolidated subsidiary, Medicago to cease operations
993 (2023). https://www.mcgc.com/english/news_release/pdf/01468/01708.pdf [Accessed May 21, 2018].
994
995 Munoz C, Schröder K, Henes B, Hubert J, Leblond S, Poigny S, Reski R, Wandrey F. Phytochemical
996 exploration of ceruchinol in moss: A multidisciplinary study in biotechnological cultivation of
997 *Physcomitrium patens* (Hedw.) Mitt. Appl Sci (2024) 14:1274. doi: 10.3390/app14031274
998
999 Mori S, Ozaki S, Yasugi T, Yoshikawa H, Taketani Y, Kanda. Inhibitory cis-element-mediated decay of
1000 human papillomavirus type 16 L1-transcript in undifferentiated cells. Mol Cell Biochem (2006) 288:47–57.
1001 doi: 10.1007/s11010-006-9117-7
1002

1003 Mortola E, Roy P. Efficient assembly and release of SARS coronavirus-like particles by a heterologous
1004 expression system. FEBS Lett (2004) 576:174–178. doi: 10.1016/J.FEBSLET.2004.09.009
1005
1006 Murén E, Nilsson A, Ulfstedt M, Johansson M, Ronne H. Rescue and characterization of episomally
1007 replicating DNA from the moss *Physcomitrella*. Proc Nat Acad Sci USA (2009) 106:19444–49. doi:
1008 10.1073/pnas.0908037106
1009
1010 Muthamilselvan T, Khan MRI, Hwang I. Assembly of human papillomavirus 16 L1 protein in *Nicotiana*
1011 *benthamiana* chloroplasts into highly immunogenic Virus-Like Particles. J Plant Biol (2023) 66:331–340.
1012 doi: 10.1007/s12374-023-09393-6
1013
1014 Naupu PN, van Zyl AR, Rybicki EP, Hitzeroth II. Immunogenicity of plant-produced human papillomavirus
1015 (HPV) virus-like particles (VLPs). Vacc (2020) 8:740. doi: 10.3390/VACCINES8040740
1016
1017 Niederkrüger H, Busch A, Dabrowska-Schlepp P, Krieghoff N, Schaaf A, Frischmuth T. „Single-use
1018 processing as a safe and convenient way to develop and manufacture moss-derived biopharmaceuticals".
1019 In: Eibl R, Eibl D, editors. Single-use technology in biopharmaceutical manufacture, 2nd edition. Hoboken
1020 NJ: Wiley (2019). p.311-318. https://doi.org/10.1002/9781119477891.ch28
1021
1022 Nooraei S, Bahrulolum H, Hoseini ZS, Katalani C, Hajizade A, Easton AJ, Ahmadian G. Virus-like particles:
1023 preparation, immunogenicity and their roles as nanovaccines and drug nanocarriers. J Nanobiotech (2021)
1024 19:59. doi: 10.1186/s12951-021-00806-7
1025
1026 Orellana-Escobedo L, Rosales-Mendoza S, Romero-Maldona A, Parsons J, Decker EL, Monreal-Escalante E,
1027 Moreno-Fierros L, Reski R. An Env-derived multi-epitope HIV chimeric protein produced in the moss
1028 *Physcomitrella patens* is immunogenic in mice. Plant Cell Rep (2015) 34:425-433. doi: 10.1007/s00299-
1029 014-1720-6
1030
1031 Park MA, Kim HJ, Kim HJ. Optimum conditions for production and purification of human papillomavirus
1032 type 16 L1 protein from *Saccharomyces cerevisiae*. Prot Expr Pur (2008) 59:175–181. doi:
1033 10.1016/j.pep.2008.01.021
1034

1035 Parsons J, Altmann F, Arrenberg CK, Koprivova A, Beike AK, Stemmer C, Gorr G, Reski R, Decker EL. Moss-
1036 based production of asialo-erythropoietin devoid of Lewis A and other plant-typical carbohydrate
1037 determinants. Plant Biotech J (2012) 10:851–861. doi: 10.1111/J.1467-7652.2012.00704.X
1038
1039 Peng W, Rayaprolu V, Parvate AD, Proner MF, Hui S, Parekh D, Shaffer K, Yu X, Saphire EO, Snijder J. Glycan
1040 shield of the ebolavirus envelop glycoprotein GP. Comm Biol (2022) 5:785. doi: 10.1038/s42003-022-
1041 03767-1
1042
1043 Pineo CB, Hitzeroth II, Rybicki EP. Immunogenic assessment of plant-produced human papillomavirus type
1044 16 L1/L2 chimaeras. Plant Biotech J (2013) 11:964–975. https://doi.org/10.1111/pbi.12089
1045
1046 Ramezaniaghdam M, Bohlender LL, Parsons J, Hoernstein SNW, Decker EL, Reski R. Recombinant
1047 production of spider silk protein in Physcomitrella photobioreactors. Plant Cell Rep (2025) 44:103. doi:
1048 10.1007/s00299-025-03485-y
1049
1050 Rempfer C, Wiedemann G, Schween G, Kerres KL, Lucht JM, Horres R, Decker EL, Reski R.
1051 Autopolyploidization affects transcript patterns and gene targeting frequencies in Physcomitrella. Plant
1052 Cell Rep (2022) 41:153-173. doi: 10.1007/s00299-021-02794-2
1053
1054 Reski R. Development, genetics and molecular biology of mosses. Bot Acta (1998) 111:1–15. doi:
1055 10.1111/j.1438-8677.1998.tb00670.x
1056
1057 Reski R. Quantitative moss cell biology. Curr Op Plant Biol (2018) 46:39–47. doi:
1058 10.1016/J.PBI.2018.07.005
1059
1060 Reski R, Abel WO. Induction of budding on chloronemata and caulonemata of the moss, *Physcomitrella*
1061 *patens*, using isopentenyladenine. Planta (1985) 165:354-358. doi: 1007/BF00392232
1062
1063 Reski R, Parsons J, Decker EL. Moss-made pharmaceuticals: from bench to bedside. Plant Biotech J (2015)
1064 13:1191–98. doi: 10.1111/pbi.12401
1065

1066 Reski R, Bae H, Simonsen HT. *Physcomitrella patens*, a versatile synthetic biology chassis. Plant Cell Rep
1067 (2018) 37:1409–17. doi: 10.1007/S00299-018-2293-6
1068
1069 Roden RBS, Stern PL. Opportunities and challenges for human papillomavirus vaccination in cancer. Nat
1070 Rev Cancer (2018) 18:240-254. doi: 10.1038/nrc.2018.13
1071
1072 Rommel O, Dillner J, Fligge C, Bergsdorf C, Wang X, Selinka HC, Sapp M. Heparan sulfate proteoglycans
1073 interact exclusively with conformationally intact HPV L1 assemblies: Basis for a virus-like particle ELISA. J
1074 Med Virol (2005) 75:114–121. doi: 10.1002/jmv.20245
1075
1076 Rosales-Mendoza S, Orellana-Escobedo L, Romero-Maldonado A, Decker EL, Reski R. The potential of
1077 *Physcomitrella patens* as a platform for the production of plant-based vaccines. Exp Rev Vacc (2014)
1078 13:203-212. doi: 10.1586/14760584.2014.872987
1079
1080 Ross TM, Mahmood K, Crevar CJ, Schneider-Ohrum K, Heaton PM, Bright RA. A trivalent virus-like particle
1081 vaccine elicits protective immune responses against seasonal influenza strains in mice and ferrets. PLOS
1082 ONE (2009) 4:e6032. doi: 10.1371/JOURNAL.PONE.0006032
1083
1084 Ruiz-Molina N, Parsons J, Müller M, Hoernstein SNW, Bohlender LL, Pumple S, Zipfel PF, Häffner K, Reski
1085 R, Decker EL. A synthetic protein as efficient multitarget regulator against complement over-activation.
1086 Comm Biol (2022a) 5:152. doi: 10.1038/s42003-022-03094-5
1087
1088 Ruiz-Molina N, Parsons J, Schroeder S, Posten C, Reski R, Decker EL. Process engineering of
1089 biopharmaceutical production in moss bioreactors *via* model-based description and evaluation of
1090 phytohormone impact. Front Bioeng Biotech (2022b) 10:837965. doi: 10.3389/fbioe.2022.837965
1091
1092 Rybicki EP. Plant molecular farming of virus-like nanoparticles as vaccines and reagents. WIREs Nanomed
1093 Nanobiotech (2020) 12:e1587. doi: 10.1002/wnan.1587
1094
1095 Sapp M, Fligge C, Petzak I, Robin Harris J, Streeck RE. Papillomavirus assembly requires trimerization of
1096 the major capsid protein by disulfides between two highly conserved cysteines. J Virol (1998) 72:6186-
1097 6189. doi: 10.1128/jvi.72.7.6186-6189.1998

1098

1099 Schmidt CQ, Slingsby FC, Richards A, Barlow PN. Production of biologically active complement factor H in
1100 therapeutically useful quantities. Prot Expr Pur (2011) 76:254–263. doi: 10.1016/J.PEP.2010.12.002
1101

1102 Schween G, Hohe A, Koprivova A, Reski R. Effects of nutrients, cell density and culture techniques on
1103 protoplast regeneration and early protonema development in a moss, *Physcomitrella patens*. J Plant Phys
1104 (2003) 160:209-212. doi: 10.1078/0176-1617-00855
1105

1106 Scotti N, Rybicki EP. Virus-like particles produced in plants as potential vaccines. Exp Rev Vacc (2013)
1107 12:211–224. doi: 10.1586/erv.12.147
1108

1109 Serradell MC, Rupil LL, Martino RA, Prucca CG, Carranza PG, Saura A, Fernández EA, Gargantini PR, Tenaglia
1110 AH, Petiti JP, Tonelli RR, Reinoso-Vizcaino N, Echenique J, Berod L, Piaggio E, Bellier B, Sparwasser T,
1111 Klatzmann D, Luján HD (2019) Efficient oral vaccination by bioengineering virus-like particles with
1112 protozoan surface proteins. Nat Comm (2019) 10:361. doi: 10.1038/s41467-018-08265-9
1113

1114 Shen JS, Busch A, Day TS, Meng XL, Yu CI, Dabrowska-Schlepp P, Fode B, Niederkrüger H, Forni S, Chen S,
1115 Schiffmann R, Frischmuth T, Schaaf A. Mannose receptor-mediated delivery of moss-made α-
1116 galactosidase A efficiently corrects enzyme deficiency in Fabry mice. J Inher Metab Dis (2016) 39:293–303.
1117 Doi: 10.1007/S10545-015-9886-9
1118

1119 Shi L, Sanyal G, Ni A, Luo Z, Doshna S, Wang B, Graham TL, Wang N, Volkin DB. Stabilization of human
1120 papillomavirus virus-like particles by non-ionic surfactants. J Pharm Sci (2005) 94:1538–51. doi:
1121 10.1002/jps.20377
1122

1123 Shi L, Sings HL, Bryan JT, Wang B, Wang Y, Mach H, Kosinski M, Washabaugh MW, Sitrin R, Barr E.
1124 GARDASIL®: Prophylactic human papillomavirus vaccine development – From bench top to bed-side. Clin
1125 Pharm Therap (2007) 81:259–264. doi: 10.1038/SJ.CLPT.6100055
1126

1127 Šmídková M, Müller M, Thönes N, Piuko K, Angelisová P, Velemínský J, Angelis KJ. Transient expression of
1128 human papillomavirus type 16 virus-like particles in tobacco and tomato using a tobacco rattle virus
1129 expression vector. Biol Plant (2010) 54:451–460. doi: 10.1007/s10535-010-0081-4

1130

1131 Song JM, Wang BZ, Park KM, van Rooijen N, Quan FS, Kim MC, Jin HT, Pekosz A, Compans RW, Kang SM.
1132 Influenza virus-like particles containing M2 induce broadly cross protective immunity. PLOS ONE (2011)
1133 6:e14538. doi: 10.1371/JOURNAL.PONE.0014538

1134

1135 Studentsov YY, Schiffman M, Strickler HD, Ho GYF, Pang YYs, Schiller J, Herrero R, Burk RD. Enhanced
1136 enzyme-linked immunosorbent assay for detection of antibodies to virus-like particles of human
1137 papillomavirus. J Clin Microbiol (2002) 40:1755-60. doi: 10.1128/JCM.40.5.1755-1760.2002

1138

1139 Strepp R, Scholz S, Kruse S, Speth V, Reski R. Plant nuclear gene knockout reveals a role in plastid division
1140 for the homolog of the bacterial cell division protein FtsZ, an ancestral tubulin. Proc Nat Acad Sci USA
1141 (1998) 95:4368–73. doi: 10.1073/PNAS.95.8.4368

1142

1143 Top O, Parsons J, Bohlender LL, Michelfelder S, Kopp P, Busch-Steenberg C, Hoernstein SNW, Zipfel PF,
1144 Häffner K, Reski R, Decker EL. Recombinant production of MFHR1, a novel synthetic multitarget
1145 complement inhibitor, in moss bioreactors. Front Plant Sci (2019) 10:260. doi: 10.3389/FPLS.2019.00260

1146

1147 Top O, Milferstaedt SWL, van Gessel N, Hoernstein SNW, Özdemir B, Decker EL, Reski R. Expression of a
1148 human cDNA in moss results in spliced mRNAs and fragmentary protein isoforms. Comm Biol (2021) 4:964.
1149 doi: 10.1038/s42003-021-02486-3

1150

1151 Torresi J. The rationale for a preventative HCV virus-like particle (VLP) vaccine. Front Microbiol (2017)
1152 8:2163. doi: 10.3389/fmicb.2017.02163

1153

1154 van Wijk KJ. Intra-chloroplast proteases: A holistic network view of chloroplast proteolysis. Plant Cell
1155 (2024) 36:3116–30. https://doi.org/10.1093/plcell/koae178

1156

1157 Varsani A, Williamson AL, Rose RC, Jaffer M, Rybicki EP. Expression of Human papillomavirus type 16
1158 major capsid protein in transgenic *Nicotiana tabacum* cv. Xanthi. Arch Virol (2003) 148:1771–86. doi:
1159 10.1007/s00705-003-0119-4

1160

1161 Weise A, Rodriguez-Franco M, Timm B, Hermann M, Link S, Jost W, Gorr G. Use of *Physcomitrella patens*
1162 actin 5' regions for high transgene expression: importance of 5' introns. Appl Microbiol Biotech (2006)
1163 70:337–345. doi: 10.1007/s00253-005-0087-6
1164
1165 Welsch S, Müller B, Kräusslich HG. More than one door - Budding of enveloped viruses through cellular
1166 membranes. FEBS Lett (2007) 581:2089–97. doi: 10.1016/J.FEBSLET.2007.03.060
1167
1168 Wiedemann G, van Gessel N, Köchl F, Hunn L, Schulze K, Maloukh L, Nogué F, Decker EL, Hartung F, Reski
1169 R. RecQ helicases function in development, DNA repair, and gene targeting in *Physcomitrella patens*. Plant
1170 Cell (2018) 30:717–736. doi: 10.1105/tpc.17.00632
1171
1172 World Health Organization. Considerations for human papillomavirus (HPV) vaccine product choice
1173 (2024). https://iris.who.int/bitstream/handle/10665/376546/9789240089167-eng.pdf [Accessed May
1174 21, 2025].
1175
1176 Wu M, Huang H, Tang Y, Ren X, Jiang X, Tian M, Li W. Unveiling the multifaceted realm of human
1177 papillomavirus: a comprehensive exploration of biology, interactions, and advances in cancer
1178 management. Front Immunol (2024) 15:1430544. doi: 10.3389/fimmu.2024.1430544
1179
1180 Zahin M, Joh J, Khanal S, Husk A, Mason H, Warzecha H, Ghim SJ, Miller DM, Matoba N, Jenson AB. Scalable
1181 production of HPV16 L1 protein and VLPs from tobacco leaves. PLOS ONE (2016) 11:e 0160995. doi:
1182 10.1371/JOURNAL.PONE.0160995
1183
1184 Zhang S, Yong LK, Li D, Cubas R, Chen C, Yao Q. Mesothelin virus-like particle immunization controls
1185 pancreatic cancer growth through CD8+ T cell induction and reduction in the frequency of CD4+ foxp3+
1186 ICOS- regulatory T cells. PLOS ONE (2013) 8:e68303 doi: 10.1371/JOURNAL.PONE.0068303
1187
1188 Zhao X, Schwartz S. Inhibition of HPV-16 L1 expression from L1 cDNAs correlates with the presence of
1189 hnRNP A1 binding sites in the L1 coding region. Virus Genes (2008) 36:45–53. doi: 10.1007/s11262-007-
1190 0174-0
1191

1192 Zlotnick A, Mukhopadhyay S. Virus assembly, allostery and antivirals. Trends Microbiol (2011) 19:14–
1193 23.doi: 10.1016/J.TIM.2010.11.003
1194
1195 zur Hausen H (2002) Papillomaviruses and cancer: From basic studies to clinical application. Nat Rev
1196 Cancer (2002) 2:342-350. doi: 10.1038/nrc798
1197
1198 zur Hausen H, de Villiers EM, Gissmann L. Papillomavirus infections and human genital cancer. Gyn Oncol
1199 (1081) 12:S124–S128. doi 10.1016/0090-8258(81)90067-6

1200 # Supplementary Information

1201 **Supplementary Figure S1 – Vector maps**

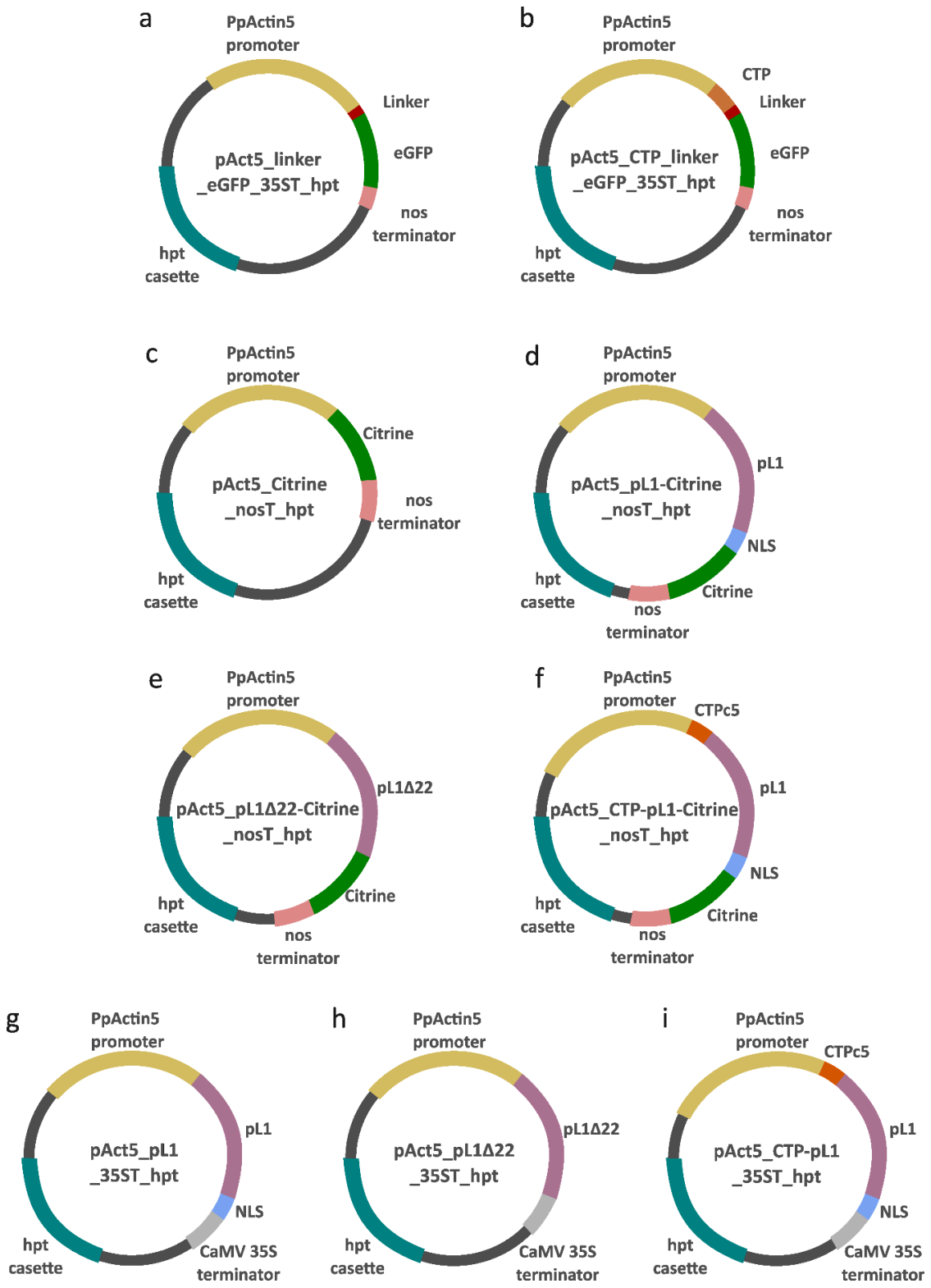

1202

1203 **List of all vectors used in this study.** Vectors **a** & **b** were used for the characterization of chloroplast transit
1204 peptides (CTPs). Vector **a** served as a control and was used as a cloning template for inserting different
1205 CTP candidates. Vectors **c**, **d**, **e** & **f** were used for the analysis of L1 subcellular targeting. Vector **c** served
1206 as a control and was used as a cloning template for inserting either pL1, pL1Δ22 or CTP-pL1 CDS (**d**, **e** & **f**,
1207 respectively). Vectors **g**, **h** & **i** were used for generation of stable transgenic Physcomitrella lines. The
1208 vectors contain either the full length pL1 including the native nuclear localization signal (NLS) (**g**), a
1209 truncated version lacking the NLS (**h**), or the full-length version including the native NLS and an N-terminal
1210 chloroplast transit peptide (**i**). All vectors contain the PpActin5 promoter (yellow), the CaMV 35S
1211 terminator (grey), and a hygromycin (hpt)(turquoise) resistance cassette for selection. Other elements are
1212 the GGGGGA linker (red), CTP (orange), NLS (blue) and eGFP or Citrine (green). Genetic elements are not
1213 depicted true to scale. Vector sizes: 7260 bp (**a**), 7461 bp (**b**), 7299 bp (**c**), 8802 bp (**d**), 8736 bp (**e**), 9021
1214 bp (**f**), 7998 bp (**g**), 7932 bp (**h**), 8217 bp (**i**).

Supplementary Figure S2 - Generation of Physcomitrella-optimized (p)L1

HPV-16 hL1

ATGTCCCTGTGGCTGCCCAGCGAGGCCACCGTGTACCTGCCCCCCGTGCCCGTGAGCAAGGTGGTGAGCACCGATGAGTACGTGGCCCGGA
CCAACATCTACTACCACGCCGGCACCTCCAGACTGCTGGCCGTGGGCCACCCCTACTTCCCCATCAAGAAGCCCAACAACAACAAGATCCTGG
TGCCCAAGGTGAGCGGCCTGCAATACCGGGTGTTCAGAATCCACCTGCCCGACCCCAATAAGTTCGGCTTCCCCGACACCAGCTTCTACAACC
CCGACACCCAGAGACTGGTGTGGGCCTGCGTGGGCGTGGAGGTGGGCAGAGGCCAGCCTCTGGGCGTGGGCATCAGCGGCCACCCTCTGC
TGAACAAGCTGGACGACACCGAGAACGCCAGCGCCTACGCCGCCAACGCCGGCGTGGATAACAGAGAATGCATCAGCATGGACTACAAGCA
GACCCAGCTGTGCCTCATCGGCTGCAAGCCCCCCATCGGCGAGCACTGGGGCAAGGGCAGCCCCTGCACCAACGTGGCCGTGAATCCTGGC
GACTGTCCTCCCCTGGAACTCATCAACACCGTGATCCAGGACGGCGACATGGTGGACACCGGCTTCGGCGCCATGGACTTCACCACCCTCCAG
GCCAATAAGAGCGAGGTGCCCCTGGACATCTGCACCAGCATCTGCAAGTACCCCGACTACATCAAGATGGTGAGCGAGCCCTACGGCGATAG
CCTGTTCTTCTACCTGCGGCGGGAGCAGATGTTCGTGCGGCACCTGTTCAACAGAGCCGGCGCCGTGGGCGAGAACGTGCCCGACGACCTGT
ACATCAAGGGCAGCGGCAGCACCGCCAACCTGGCCAGCAGCAACTACTTCCCTACCCCCAGCGGCTCCATGGTGACCAGCGACGCCCAGATC
TTCAACAAGCCCTACTGGCTCCAGAGAGCCCAGGGCCACAACAATGGCATCTGCTGGGGCAACCAGCTGTTCGTGACCGTGGTGGATACCAC
CCGGAGCACCAACATGTCCCTGTGCGCCGCCATCAGCACCAGCGAGACCACCTACAAGAACACCAACTTCAAGGAGTACCTGAGGCACGGCG
AGGAGTACGACCTCCAGTTCATCTTCCAGCTGTGCAAGATCACCCTCACCGCCGACGTGATGACCTACATCCACAGCATGAACAGCACCATCC
TGGAGGACTGGAACTTCGGCCTGCAGCCCCCTCCTGGCGGCACCCTGGAGGACACCTACAGATTCGTGACCAGCCAGGCCATCGCATGCCAG
AAGCACACCCCTCCCGCCCCTAAGGAGGACCCCCTGAAGAAGTACACCTTCTGGGAGGTGAACCTGAAGGAGAAGTTCAGCGCCGACCTGG
ACCAGTTCCCTCTGGGCAGAAAGTTCCTGCTGCAAGCCGGCCTGAAGGCCAAGCCTAAGTTCACCCTGGGCAAGAGAAAGGCCACCCCCACC
ACAAGCAGCACCAGCACCACCGCCAAGCGGAAGAAGCGCAAGCTGTGA

HPV-16 pL1

ATGTCCCTGTGGCTGCCCAGCGAGGCCACCGTGTACCTGCCCCCCGTGCCCGTGAGCAAAGTGGTGAGCACCGATGAGTACGTGGCCCGGAC
CAACATCTACTACCACGCCGGCACCTCCAGACTGCTGGCCGTGGGCCACCCCTACTTCCCCATCAAGAAGCCCAACAACAACAAGATCCTGGT
GCCCAAAGTGAGCGGCCTGCAGTACCGGGTGTTCAGAATCCACCTGCCCGACCCCAACAAGTTCGGCTTCCCCGACACCAGCTTCTACAACCC
CGACACCCAGAGACTGGTGTGGGCCTGCGTGGGCGTGGAAAGTGGGCAGAGGCCAGCCTCTGGGCGTGGGCATCAGCGGCCACCCTCTGCT
GAACAAGCTGGACGACACCGAGAACGCCAGCGCCTACGCCGCCAACGCCGGCGTGGATAACAGAGAGTGCATCAGCATGGACTACAAGCA
GACCCAGCTGTGCCTCATCGGCTGCAAGCCCCCCATCGGCGAGCACTGGGGCAAGGGCAGCCCCTGCACCAACGTGGCCGTGAACCCTGGC
GACTGCCCTCCCCTGGAGCTCATCAACACCGTGATCCAGGACGGCGACATGGTGGACACCGGCTTCGGCGCCATGGACTTCACCACCCTCCA
GGCCAACAAGAGCGAAGTGCCCCTGGACATCTGCACCAGCATCTGCAAGTACCCCGACTACATCAAGATGGTGAGCGAGCCCTACGGCGATA
GCCTGTTCTTCTACCTGCGGCGCGAGCAAATGTTTGTGCGGCACCTGTTCAACAGAGCCGGCGCCGTGGGCGAGAACGTGCCCGACGACCTG
TACATCAAGGGCAGCGGCAGCACCGCCAACCTGGCCAGCAGCAACTACTTCCCTACCCCCAGCGGCTCCATGGTGACCAGCGACGCCCAGAT
CTTCAACAAGCCCTACTGGCTCCAGAGAGCCCAGGGCCACAACAACGGCATCTGCTGGGGCAACCAGCTGTTCGTGACCGTGGTGGATACCA
CCCGGAGCACCAACATGTCCCTGTGCGCCGCCATCAGCACCAGCGAGACCACCTACAAGAACACCAACTTCAAGGAGTACCTGAGGCACGGC
GAGGAGTACGACCTCCAGTTCATCTTCCAGCTGTGCAAGATCACCCTCACCGCCGACGTGATGACCTACATCCACAGCATGAACAGCACCATC
CTGGAGGACTGGAACTTCGGCCTGCAGCCCCCTCCTGGCGGCACCCTGGAGGACACCTACAGATTCGTGACCAGCCAGGCCATCGCATGCCA
GAAGCACACCCCTCCCGCCCCTAAGGAGGACCCCCTGAAGAAGTACACCTTCTGGGAAAGTGAACCTGAAGGAGAAGTTCAGCGCCGACCTG
GACCAGTTCCCTCTGGGCAGAAAGTTCCTGCTGCAGGCCGGCCTGAAGGCCAAGCCTAAGTTCACCCTGGGCAAGAGAAAGGCCACCCCCAC
CACAAGCAGCACCAGCACCACCGCCAAGCGGAAGAAGCGCAAGCTGTGA

1253 **Human codon-optimized HPV-16 (h)L1 CDS and Physcomitrella-optimized HPV-16 (p)L1 CDS.** Grey
1254 marked nucleotides were changed in HPV-16 pL1 through codon usage optimization by the tool physCO
1255 (Top et al., 2021). Turquoise marked motifs refer to the Physcomitrella alternative splicing recognition
1256 sites. The green marked segment refers to a predicted miRNA binding site identified by the tool
1257 psRNATarget (Dai and Zhao, 2011; Dai et al., 2018). Light orange colored segments represent the nuclear
1258 localization signal. Nucleotide changes are underlined in the HPV-16 pL1 sequence. (hL1, GenBank
1259 accession number DQ067889; Maclean et al., 2007).

1260 **Supplementary Figure S3 - Characterization of CTPs by analysis of subcellular eGFP localization**

1261

1262

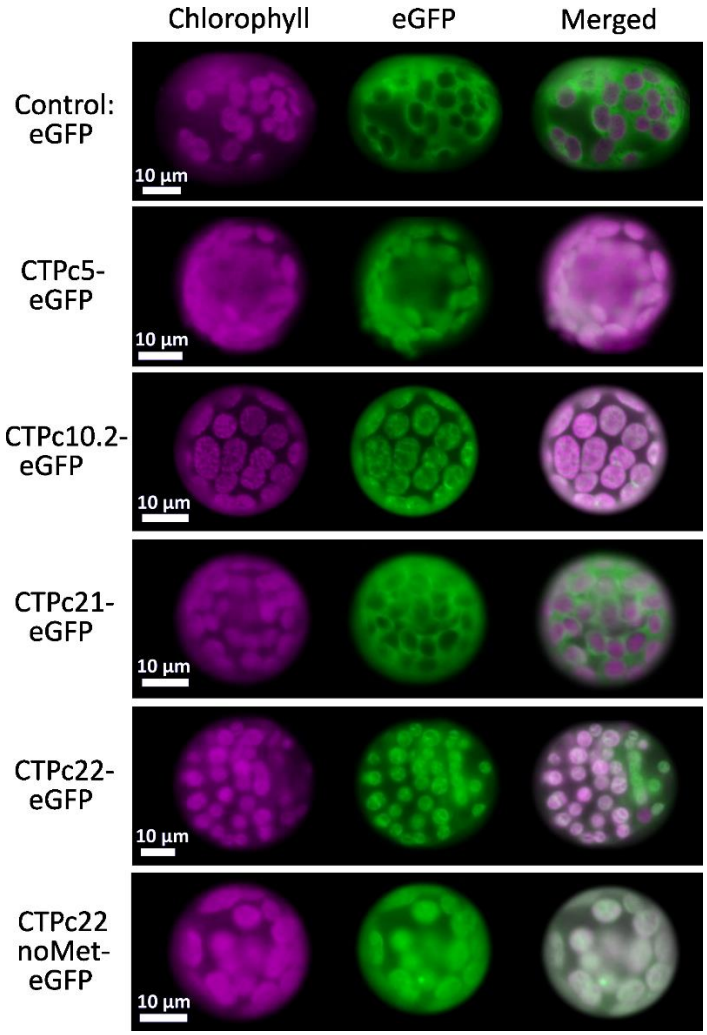

1263

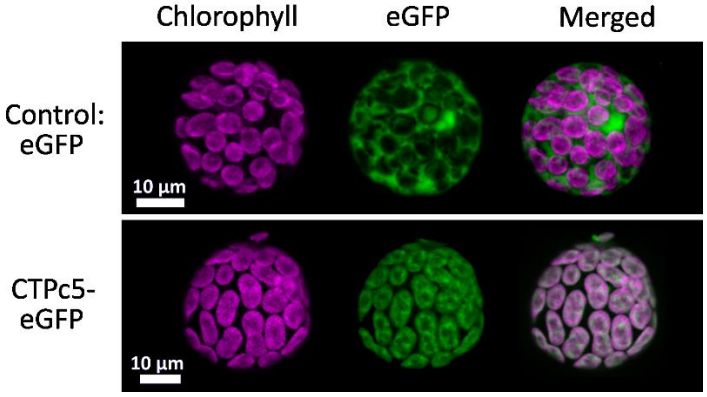

1264

1265

1266 **Microscopy pictures of Physcomitrella protoplasts transformed with CTP-eGFP constructs.** Samples
1267 were analyzed using a rhodamine and a FITC filter to identify chloroplast (magenta) and eGFP localization,
1268 respectively, as well as a merge of the two signals. For sample CTPc21-eGFP no eGFP signal could be
1269 observed in chloroplasts. For samples CTPc5-eGFP, CTPc10-eGFP, CTPc22-eGFP and CTPc22noMet-eGFP
1270 green fluorescence signal is observed in chloroplasts. eGFP lacking a CTP localized to the cytoplasm and
1271 served as a negative control. The experiment was repeated two times. CTPc5 was examined a third time
1272 using confocal microscopy. Scale bars represent 10 µm.

1273 **Supplementary Figure S4 – Analysis of CDS integrity in L1-producing lines**

1274

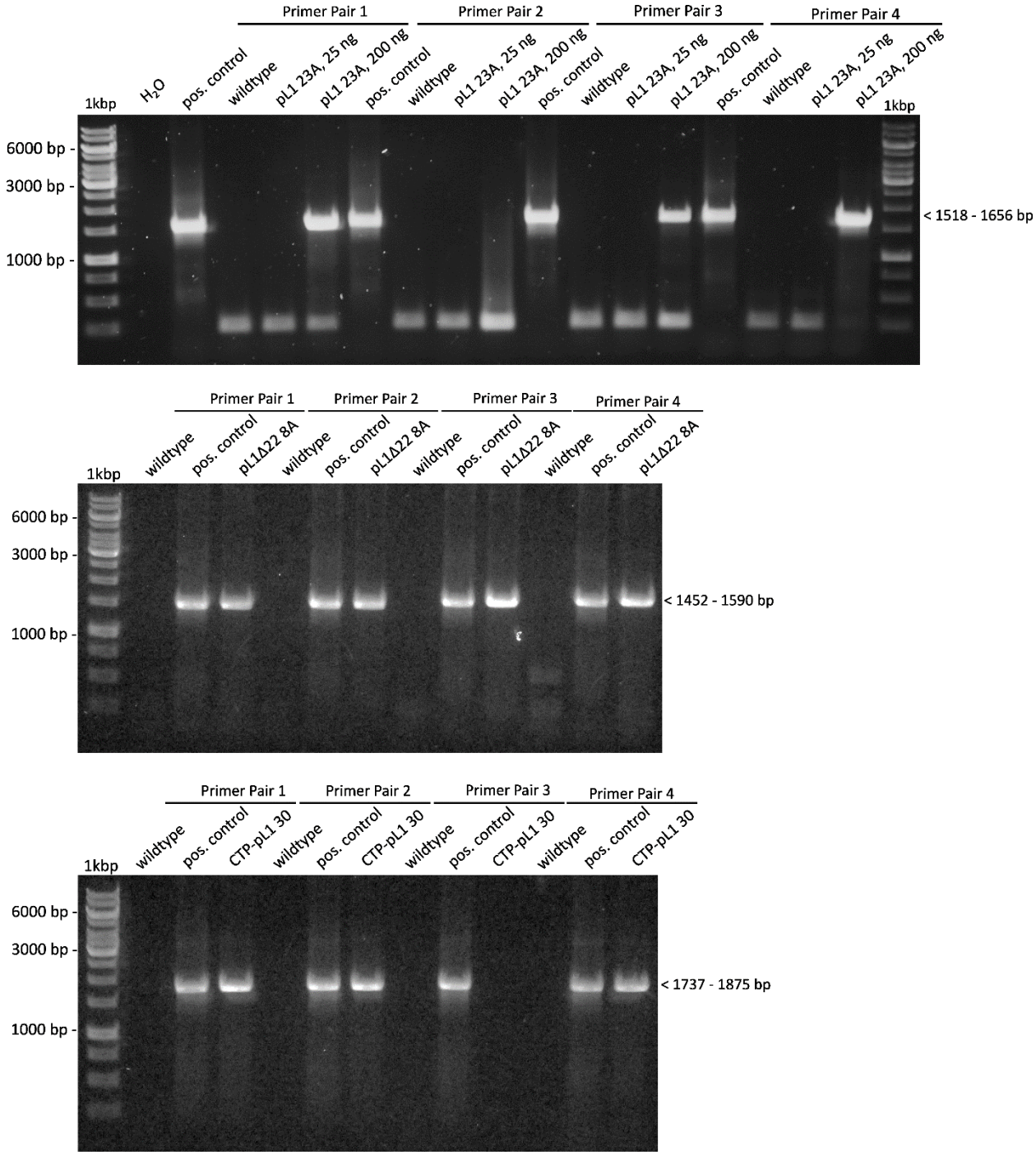

1275

1276

1277 **Analysis of rearrangements in the pL1 CDS using RT PCR.** Lines pL1 23A, pL1Δ22 8A and CTP-pL1 30 were

1278 checked for DNA or RNA rearrangements by performing PCR on cDNA using four different primer pairs.

1279 Primer pairs were selected to amplify the entire cDNA. The forward primer binds at the start codon and

1280 is the same in each primer pair (pL1_fwd_1 for lines pL1 23A & pL1Δ22 8A, CTP_pL1_fwd_1 for line CTP-
1281 pL1 30). The reverse primers are different in each pair and bind at the 3' end of the CDS or within the
1282 terminator (**Supplementary Table S1**). For line pL1 23A usage of 25 ng or 200 ng cDNA in PCR reactions
1283 was compared. Following experiments used 200 ng. Absence of distinct bands of a size smaller than the
1284 expected size is indicative for no larger rearrangements on both DNA and RNA level. No amplicon is visible
1285 for lines pL1 23A using Primer Pair 2 and CTP-pL1 30 using Primer Pair 3. The constructs used for
1286 transformation of Physcomitrella protoplasts (**Supplementary Figure S1 g - i**) served as a positive control.
1287

1288 **Supplementary Figure S5 – Analysis of the effect of reducing agents on L1 band patterning**

1289

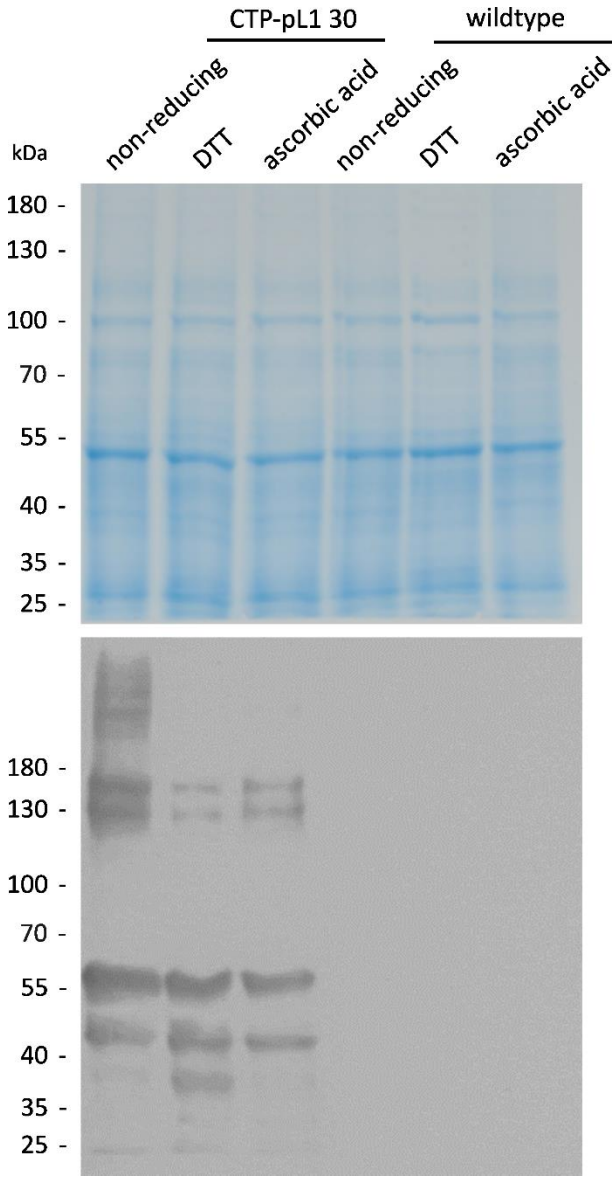

1290

1291

1292 **Analysis of the effect of reducing agents on L1 band patterning in western blots.** Samples of line CTP-
1293 pL1 30 and wildtype were extracted without reducing agent, with 50 mM DTT or 40 mM ascorbic acid.
1294 The proteins for the western blot were separated on a 7.5% TGS polyacrylamide gel under reducing
1295 conditions (5 mM DTT) before being transferred to a membrane and developed using CamVir1 antibody
1296 (1:5000).

1297

1298 **Supplementary Figure S6 – Comparison of biomass accumulation rates**

1299

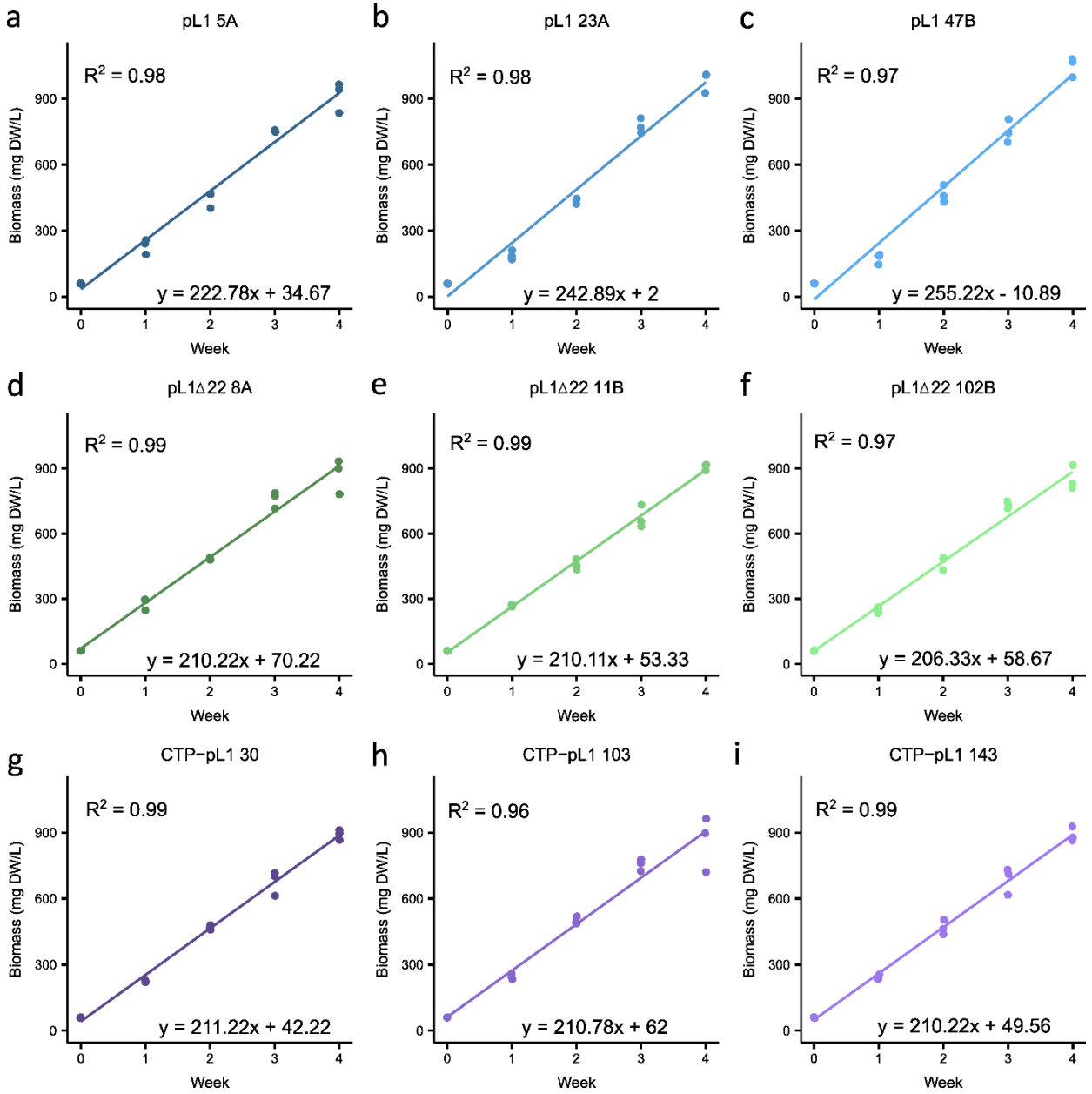

1300

1301 **Analysis of biomass accumulation rates among nine Physcomitrella lines of three different constructs.**

1302 Biomass accumulation rates were observed over a course of 4 weeks for lines pL1 5A, pL1 23A, pL1 47B

1303 (blue); pL1Δ22 8A, pL1Δ22 11B, pL1Δ22 102B (green) and CTP-pL1 30, CTP-pL1 103, CTP-pL1 143 (purple).

1304 The data was plotted using linear regression analysis and all slopes were analysed using ANOVA and post

1305 hoc multiple comparisons test (TukeyHSD). Comparison of the slopes between the constructs of pL1,

1306 pL1Δ22 and CTP-pL1 showed pL1 lines accumulated biomass faster than pL1Δ22 ($p = <0.0001$) and CTP-

1307 pL1 ($p = 0.0001$) lines. Per week $n = 3$ biological samples were taken.

1308 **Supplementary Figure S7 – Ammonium sulfate precipitation**

1309

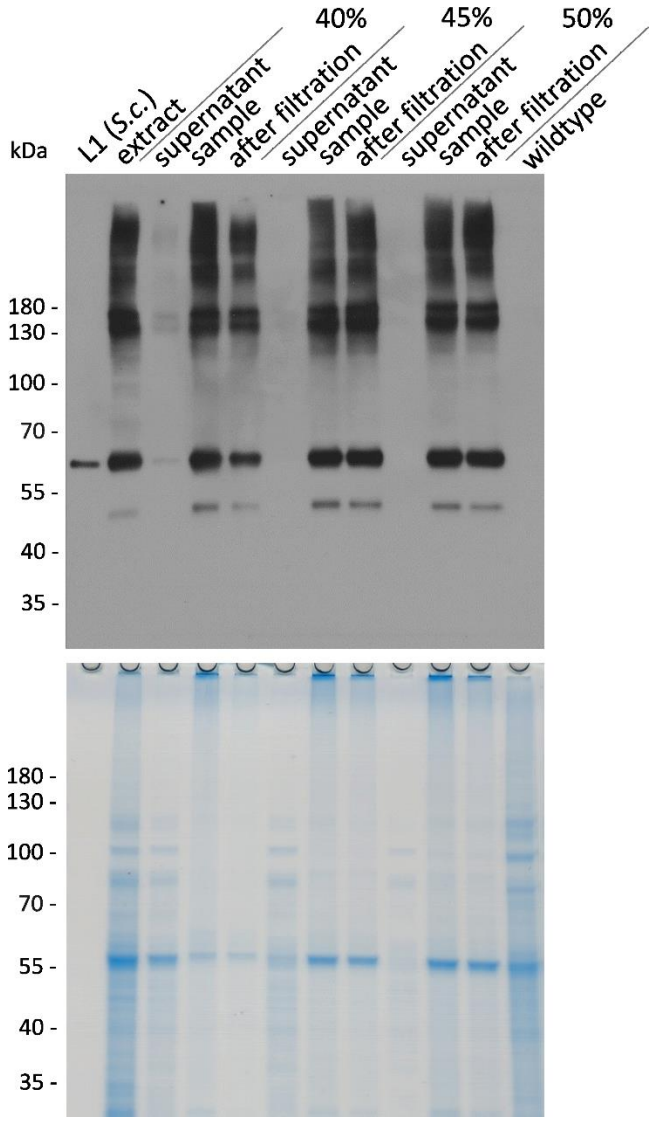

1310

1311

1312 **Ammonium sulfate precipitation of L1 from moss extracts.** Samples from the supernatant and the
1313 resuspended and dialyzed pellet before and after filtration were analyzed for the presence of L1 content
1314 and residual host proteins under reducing conditions *via* western blot and Coomassie-stained gel,
1315 respectively. CTP-pL1 30 extracts were precipitated with either 40%, 45%, or 50% (w/v) ammonium sulfate
1316 (AMS). After centrifugation, the supernatant and the precipitate were taken up and dialyzed against cation
1317 exchange chromatography binding buffer to remove excess AMS. Non-dissolved protein was cleared from
1318 the sample using 0.22 µm filters. 45% AMS was found to be sufficient for full precipitation of L1 from

1319 crude extracts. 30 ng *S. cerevisiae*-produced L1 served as a positive control and Physcomitrella wildtype
1320 as a negative control.
1321

1322 **Supplementary Figure S8 – Chromatogram of Cation Exchange purification**

1323

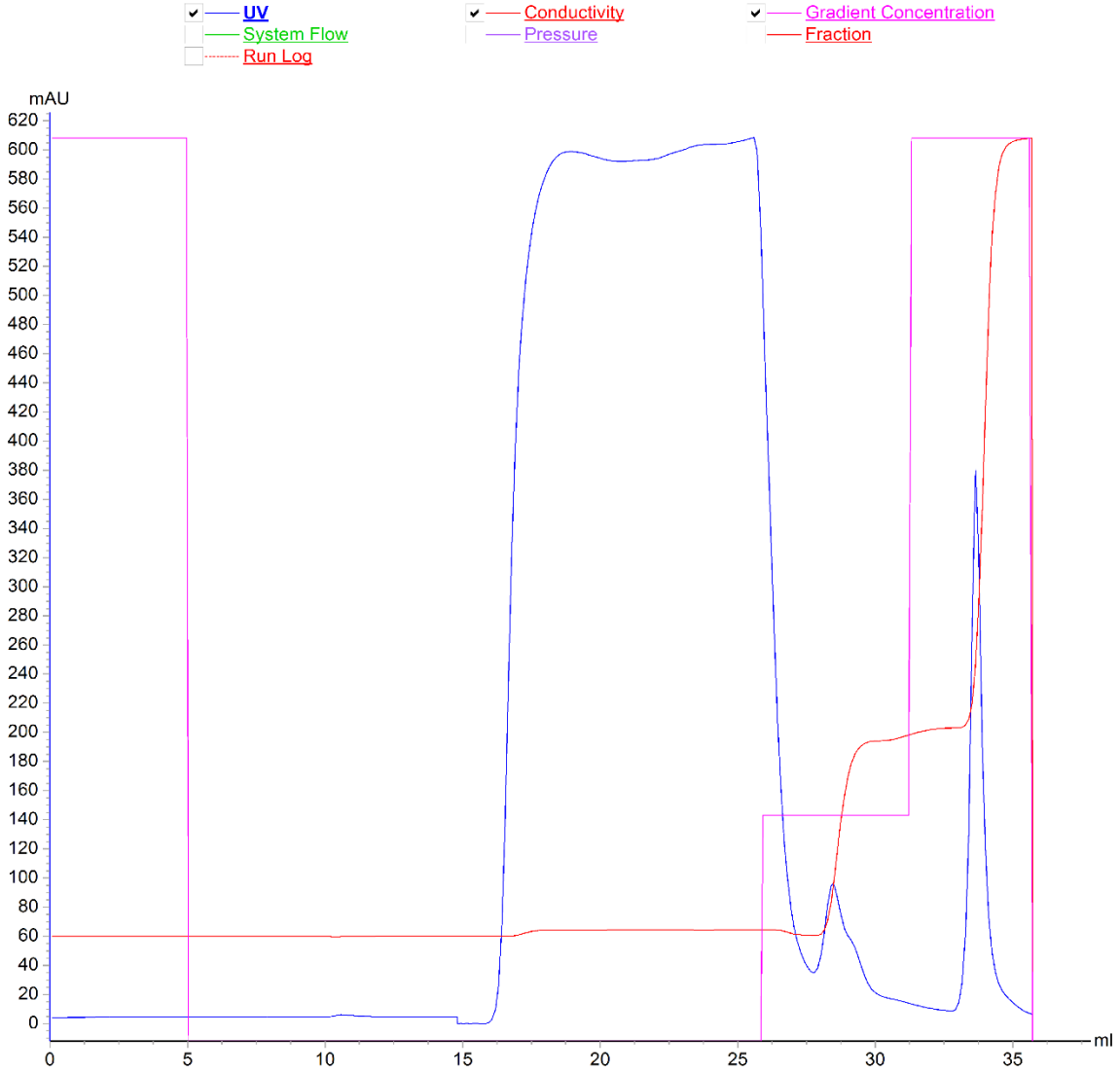

1324

1325

1326 **Chromatogram of HPV-16 L1 purification from moss using cation exchange chromatography.** The
1327 chromatogram shows the UV absorbance, indicative for protein concentration, in blue, gradient
1328 concentration in pink, and conductivity, indicative for salt concentration, in red. The y axis depicts milli-
1329 Absorbance Units and the x axis depicts the volume in mL. The large peak between 16 – 26 mL shows the
1330 sample application or flow through, the following small peak at 28 mL the wash fraction and the larger
1331 peak at 33 – 35 mL the elution fractions.

1332 **Supplementary Table S1 – List of primers**

1333 Capital letters refer to the part of the primer binding to the template whereas lower case letters represent
1334 overhangs added to the template via PCR. Abbreviations: fwd or fw (forward), rev or rv (reverse), CTP
1335 (chloroplast transit peptide), MMEJ (micro homology-mediated end joining), GFP (green fluorescent
1336 protein), OH (overhang (lower case letters)).

1337

Primer name	Sequence (5'→3')	Application
AA2_3integFP (hpt3'seq)	ACTCGCCGATAGTGGAAACC	Amp of linker-eGFP vector part 1
PAN_PpActin-Pro_Rv	CTGCACAACAACCACCAATATTTAATTTC	Amp of linker-eGFP vector part 1
linker:EGFP_p1840_Fw	GGAGGTGGAGGTGGAGC	Amp of linker-eGFP vector part 2
HPTLUCfwd2	TTGCCCTCGGACGAGTGC	Amp of linker-eGFP vector part 2
CTP_Pp3c10_Fw	aattaaatattggtggttgttgtgcagATGGCGTTATTGGCGCGC	Amp of CTPc10
CTP_Pp3c10_Rv	gctccacctccacctccATTGGTGACCCTCAAAGGTCCAG	Amp of CTPc10
CTP_Pp3c5_Fw	aattaaatattggtggttgttgtgcagATGGCTACGATGAAGATTGCTGTGG	Amp of CTPc5
CTP_Pp3c5_Rv	gctccacctccacctccAGCTCGCACGGAGCTGTTC	Amp of CTPc5
CTP_Pp3c22_Fw	aattaaatattggtggttgttgtgcagATGCGGGCTCTCTGTGGAG	Amp of CTPc22 & CTPc22_noMet
CTP_Pp3c22_Rv	gctccacctccacctccCATAGCGACAATGCACCGTCTTC	Amp of CTPc22
CTP_Pp3c22_noMet_Rv	gctccacctccacctccAGCGACAATGCACCGTCTTCC	Amp of CTPc22_noMet
CTP_Pp3c21_Fw	aattaaatattggtggttgttgtgcagATGGCCGCCGTCGGAATG	Amp of CTPc21
CTP_Pp3c21_Rv	gctccacctccacctccGGCACGGACAGCGAACGC	Amp of CTPc21
Act5_seq	TCCACATGGCTACAGCTG	Colony PCR CTP-eGFP constructs
EGFP_NoLinker_Rev	CTTGTACAGCTCGTCCATG	Colony PCR CTP-eGFP constructs
XhoI-pL1-BamHI_fw	gtgcagctcgagATGTCCCTGTGGCTGCC	Amp of pL1 and pL1Δ22
XhoI-pL1-BamHI _Rv	tctagaggatccTCACAGCTTGCGCTTCTTCC	Amp of pL1
XhoI-pL1delta22-BamHI _Rv	tctagaggatcctcaGCCCAGGGTGAACTTAGGC	Amp of pL1Δ22
pL1_w/oATG_Fw	TCCCTGTGGCTGCCCAG	Amp of CTP-pL1 (no Start codon)

pL1_Rv_35St-OH	GACTGGTGATTTTTGCGGACTCTAG	Amp of pL1, Heterosplicing and MMEJ check of pL1 lines
CTPc5_Fw_Act5p-OH	tattggtggttgttgtgcagctcgagATGGCTACGATGAAGATTGCTGTG	Amp of CTPc5
CTPc5_Rv_pL1-OH	ctcgctgggcagccacagggaAGCTCGCACGGAGCTGTTC	Amp of CTPc5
Seq_hL1+HSP_Fw	CGTGATGACCTACATCCACAG	Colony PCR pL1 constructs
pL1_Rv_35St-OH	GACTGGTGATTTTTGCGGACTCTAG	Colony PCR pL1 constructs
pL1_fwd_1	ATGTCCCTGTGGCTGCCC	Heterosplicing and MMEJ check of pL1, pL1Δ22 lines (primer pair 1-4, forward)
pL1_rev_1	TCACAGCTTGCGCTTCTTCC	Heterosplicing and MMEJ check of pL1, CTP-pL1 lines (primer pair 1, reverse)
pL1d22_rev_1	TCAGCCCAGGGTGAACTTAGG	Heterosplicing and MMEJ check of pL1Δ22 lines (primer pair 1, reverse)
CTP-pL1_fwd_1	ATGGCTACGATGAAGATTGCTGTG	Heterosplicing and MMEJ check of CTP-pL1 lines (primer pair 1-4, forward)
pL1_Rv_35St-OH	GACTGGTGATTTTTGCGGACTCTAG	Heterosplicing and MMEJ check of pL1, pL1Δ22, CTP-pL1 lines (primer pair 2, reverse)
101_35S-T_rev	CCCTTATCTGGGAACTACTCACACATTATTCTGGA	Heterosplicing and MMEJ check of pL1, pL1Δ22, CTP-pL1 lines (primer pair 3, reverse)
3342_LdC-HATag-35ST-rev	GGGTTTCGCTCATGTGTTGAGCA	Heterosplicing and MMEJ check of pL1, pL1Δ22, CTP-pL1 lines (primer pair 4, reverse)
pL1-fwd	GCTCGAGATGTCCCTGTG	pL1(Δ22)-GFP fusion construct
pL1-rev	AGGATCCCAGCTTGCGCTTCTTC	(CTP-)pL1-GFP fusion construct
pL1d22-rev	AGGATCCGCCCAGGGTGAACTTAG	pL1Δ22-GFP fusion construct
CTPc5-pL1 fwd	GCTCGAGATGGCTACGATGA	CTP-pL1-GFP fusion construct

1338
1339

1340 **Supplementary Table S2 – Predicted chloroplast transit peptides for six selected proteins in**
1341 **Physcomitrella. The predictions were performed with TargetP-2.0; Armenteros et al. (2019).**
1342

Name: CTPc5

Protein: **Pp3c5_1370V3.1**

Predicted chloroplast transit peptide (74 aa):

MATMKIAVAAVAGTPAAAVGTRSAAATETARLCASSAQGLGLSTFVGLRAGSNASRGVTPRVRPLKAENSSVRA

Name: CTPc10.1

Protein: **Pp3c10_10490V3.1**

Predicted chloroplast transit peptide (63 aa):

MEVLPRAIATSHVVVSSSSAPKESSESGSKNNSQVSLSSVPFLRPASALAASIVSSATPAALA

Name: CTPc10.2

Protein: **Pp3c10_2940V3.1**

Predicted chloroplast transit peptide (70 aa):

MALLARGAVAAVAAVGFSNTTSKQGHQNGGSNGVLAFRGNAFCRAVAARTSSVGCQVRVKRGAGPLRVTN

Name: CTPc21

Protein: **Pp3c21_9980V3.1**

Predicted chloroplast transit peptide (43 aa):

MAAVGMTMSLKSSTALKGDFLGAALKQTVAAPKAANVAFAVRA

Name: CTPc22

Protein: **Pp3c22_5470V3.1**

Predicted chloroplast transit peptide (62 aa):

MRALCGVPSCASLSSHRLASPLLAYRACEFALGSSPGLRLEFVGRAVGLQSRSIGRRCIVAM

1343